Mathematical models of transmission dynamics and vaccine strategies in Hong Kong during the 2017 - 2018 winter influenza season

Ho, Shing Hei; He, Daihai; Eftimie, Raluca

Published in:
Journal of Theoretical Biology

DOI:
10.1016/j.jtbi.2019.05.013

Publication date:
2019

Mathematical models of transmission dynamics and vaccine strategies in Hong Kong during the 2017 - 2018 winter influenza season

Shing Hei Ho[1,*]

Faculty of Education, University of Hong Kong, Pokfulam Road, Hong Kong

Daihai He[*]

Department of Applied Mathematics, Hong Kong Polytechnic University, Hung Hom, Kowloon, Hong Kong

Raluca Eftimie[*]

Division of Mathematics, School of Science and Engineering, University of Dundee, Nethergate, Dundee, United Kingdom

Abstract

Two mathematical models described by simple ordinary differential equations are developed to investigate the Hong Kong influenza epidemic during 2017 - 2018 winter, based on overall epidemic dynamics and different influenza subtypes. The first model, describing the overall epidemic dynamics, provides the starting data for the second model which different influenza subtypes, and whose dynamics is further investigated. Weekly data from December 2017 to May 2018 are obtained from the data base of the Centre of Health Protection in Hong Kong, and used to parametrise the models. With the help of these models, we investigate the impact of different vaccination strategies and determine the corresponding critical vaccination coverage for different vaccine efficacies.

The results suggest that at least 72% of Hong Kong population should have been vaccinated during 2017 - 2018 winter to prevent the seasonal epidemic

[*]Corresponding author

Email address: shingheiho@gmail.com (Shing Hei Ho)

[1]This work was done while the author was a MSc student in the Division of Mathematics, School of Science and Engineering, University of Dundee, UK

by herd immunity (while data showed that only a maximum of 11.6% of the population were vaccinated). Our results also show that the critical vaccination coverage decreases with increasing vaccine efficacy, and the increase in one influenza subtype vaccine efficacy may lead to an increase in infections caused by a different subtype.

Keywords: Influenza, SVIR model, Vaccination coverage, Vaccine efficacy

1. Introduction

Approximately 10-20% of the world's population is infected with influenza viruses every year and it is expected that up to 15% of European population is infected by influenza in any winter season [1, 2]. The World Health Organisation (WHO) stated that annual epidemics are estimated to cause 3 to 5 million cases of severe illness and about 290 000 to 650 000 deaths worldwide [3].

Hong Kong usually experiences one or two peak seasons of influenza in one epidemic year [4]. Researches have shown that influenza season peaked at low or high temperature with high relative humidity [5]. Being a city in the subtropical region of southern China, Hong Kong experiences high humidity ($> 70\%$) throughout the year, along with low temperature in the winter ($\sim 15^{\circ}$C) and high temperature in the summer ($\sim 30^{\circ}$C) [6], which account for the two influenza peak seasons every year. The influenza season in Hong Kong usually last for two months for each period - one from January to March (winter season), the other from July to August (summer season). The high population density in Hong Kong also makes influenza easier to spread among humans, as they have a higher chance of contact with the infected individuals.

Several studies have focused on different factors affecting the influenza epidemics in Hong Kong, such as the weather [5], the change in seasonal pattern after 2009 pandemic [7], and the anti-phase synchronisation between type A viruses [8]. These studies are useful in preparing and predicting future epidemics in Hong Kong. Nonetheless, to prevent epidemics one needs to focus on vaccination and its effect can be investigated by means of mathematical models

and simulations [9].

Mathematical models are useful in investigating the dynamics and control of infectious diseases. Previous studies have examined various models for influenza epidemics in different contexts, such as the epidemics of one influenza strain [10], competitive interference between multiple influenza viral strains [11], and the cross-protective immunity between different strains [12]. Mathematical models also provide useful and inexpensive tools to test hypotheses on the optimal way to control the spread of an infection, notably through vaccination [13]. Several studies have used mathematical models to evaluate various control strategies and to design the best strategy [13, 14, 15]. However, because of the complexity of epidemics dynamics, it is still an open question to determine the best vaccine strategy for alleviating the influenza epidemics. For instance, influenza epidemics depend on multiple influenza subtypes and vaccination against only one subtype could lead to a negative impact on different subtypes [16].

This paper proposes two deterministic SVIR models based on the infection data in Hong Kong during the 2017 - 2018 winter, which are then used to investigate the effects of vaccine strategies based on vaccination coverage and vaccine efficacy against different influenza subtypes. We begin by introducing the first SVIR model (model 1) describing the overall influenza epidemic, which provides the starting data for the second SVIR model (model 2) describing the epidemic in the context of three major influenza subtypes (A_{H1}, A_{H3} and B) in Hong Kong. We parametrise the models based on the available data for the 2017 - 2018 influenza in Hong Kong. We then present the results of numerical simulations for these two models as we vary different parameters values associated with different vaccine strategies. Our work is different from the previous mathematical approaches in the literature (e.g., a SIR model with one influenza subtype [13], a SVIR model with vaccination against one influenza subtypes [15], a seasonal SEIAR model [14], and two-strains SVIR model [16]) by its use of data on the 2017 - 2018 influenza in Hong Kong and the proposal of a new mathematical model with the composite vaccine based on three influenza subtypes.

2. Mathematical Models

2.1. Epidemic Data

We obtained the data from the data base of the Centre of Health Protection in Hong Kong (CHP), which included influenza related statistics of Hong Kong [17]. Two major data sets were used in the paper:

1. Positive percentage of seasonal influenza viruses among respiratory specimens received in Laboratory (**D1**);
2. Influenza-associated hospital admission rates in public hospitals (**D2**).

Figure 1 shows both data sets from 1^{st} October 2017 to 5^{th} May 2018. Since type C viral infections remained at a steady, significantly low level, and strain C was never a dominating virus in any peak season, throughout this study (and in particular for model 2) we considered for simplicity only the type A(H1), A(H3) and B viruses.

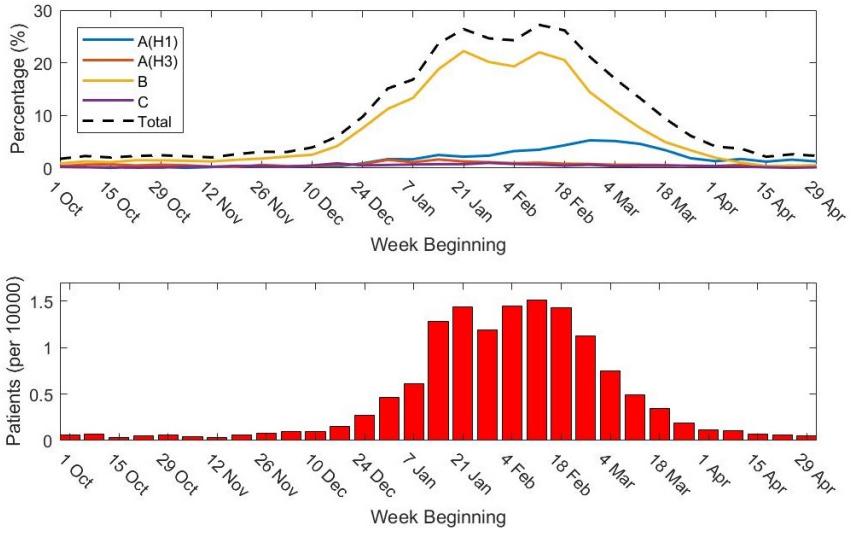

Figure 1: Surveillance data obtained from CHP from 1^{st} October 2017 to 5^{th} May 2018. (Top) Positive percentage of seasonal influenza viruses among respiratory specimens received in Laboratory (**D1**). (Bottom) Influenza-associated hospital admission rates in public hospitals (**D2**).

The influenza season of 2017 - 2018 winter was identified by CHP on the basis of influenza surveillance data. Respiratory specimens were received and tested each week by CHP to detect and distinguish the pathogens from the specimens. Once the positive detection of seasonal influenza viruses exceeded the baseline threshold of 10.7% among the specimens [18, 19], Hong Kong was considered to have entered the influenza season, while the decline on the percentage back to the baseline level marked the end of the influenza season. CHP announced that the influenza season in 2017-18 winter was detected between 7^{th} January and 31^{st} March 2018 [18, 19]. This period is denoted in the paper as the "peak season", to separate it from the annual influenza activity. In order to improve fitting accuracy, more weekly data were needed for fitting. Therefore, the period from 10^{th} December 2017 to 5^{th} May 2018 was chosen to be investigated as both data sets (D1 and D2) started to increase significantly from 10^{th} December 2017 and were maintained at a low level after the peak season. We refer to this period as the "Study Period".

Several assumptions were made for the models introduced in this study:

1. Hong Kong has an estimated population of 7.4 million [20].
2. There was no net growth rate of the population over the study period.
3. 15% of Hong Kong population was infected by influenza over the peak season.
4. Individuals only got vaccinated through the government subsiding schemes and vaccine did not wane during the period.
5. Incubation period was ignored.
6. All individuals were capable of infections at the start of the study period (including the vaccinated ones since the vaccine efficacy was lower than 100%).
7. Once recovered from infection, individuals had gained immunity against influenza and they did not get infected by influenza again during the rest of the season.
8. No cross-infection occurred, i.e. individuals did not get infected by two or more influenza subtypes at the same time or one after another.

Given the worldwide infected statistics and situation in Hong Kong (as discussed in Section 1), throughout the study we assumed that 15% of the Hong Kong population was infected during the peak season. Also, as it was generally expensive to get vaccinated and limited vaccines were available in Hong Kong, we assumed that individuals only got vaccinated via the government subsiding schemes, i.e. the number of vaccinated individuals were recorded and announced by official organisations. More information about the government vaccination programme can be obtained via the government website [21].

2.2. Vaccination

Two vaccines composed of A(H1), A(H3) and B viruses were recommended in Hong Kong during the 2017 - 2018 winter. The compositions of the vaccines can be found in Appendix A. CHP had established several vaccination schemes to provide free or subsidised seasonal influenza vaccinations to several groups of Hong Kong residents, including pregnant women, elderly, infants and children, whom are considered to have a higher risk of infection due to their low immunity [22]. We obtained the number of vaccinations from the CHP website and newsletters; these numbers are represented by the red squares in Figure 2. Note here that the vaccination numbers followed an inverse exponential decay pattern (i.e., the solution of the following equation),

$$\frac{dV}{dt} = r\left(1 - \frac{V}{A}\right) = f(V), \tag{1}$$

where r and A denote the growth rate and the maximum of vaccinated population respectively. These two parameters are estimated using the least squares method (which approximates the parameters by minimizing the square errors between the numerical curve and the data). In general, a vaccine becomes effective two weeks after the injection [23]. If the "effectively vaccinated population" is defined as those individuals who obtained effective vaccine protection, then we can use equation (1) with two weeks delay to describe the number of effectively vaccinated population. Both curves are shown in Figure 2, the blue curve describing the solution of equation (1) fitted to the data, and the orange

curve describing the solution of equation (1) shifted by two weeks (i.e. the effective vaccinated population). Note that, throughout this study we focus only on the effectively vaccinated population. (Those who have not acquired vaccine protection are still in the susceptible class).

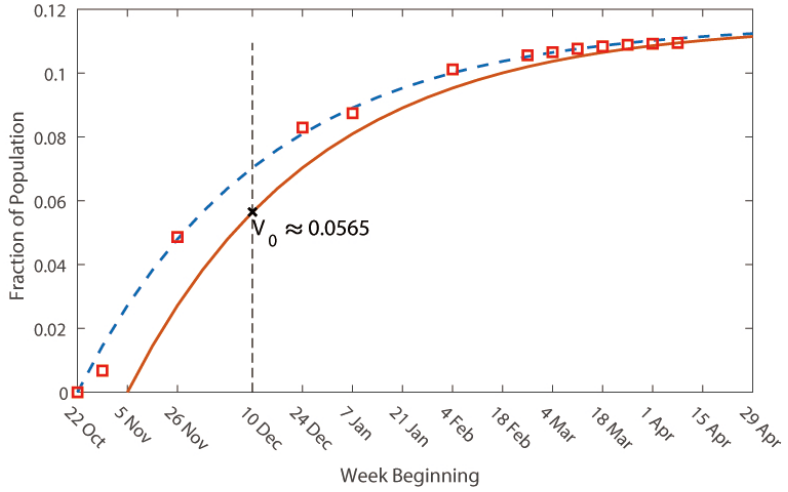

Figure 2: Vaccinated population in Hong Kong over the 2017-18 winter. The red squares and the blue curve represent the data from CHP and its fitted curve respectively. The orange curve is actually the blue curve with a 2-weeks delay to represent the effectively vaccinated population. The week beginning 10^{th} December 2017 was the start of the study period and of the peak season, and hence V_0 was chosen to be the initial value of both effectively vaccinated and vaccinated compartments over this period.

Using equation (1) and the data in Figure 2, we estimated the parameter values to $r = 0.0155$ and $A = 0.1155$ (which indicated that a maximum of $\sim 11.6\%$ population had been vaccinated by the end of the season; refer to the population size in Figure 2 on the week beginning 29 April). $V_0 \approx 0.0565$ is the initial value of both vaccinated and effectively vaccinated compartments in the models. We will discuss these compartments in Sections 2.3.1 and 2.4.1. This V_0 value was chosen by focusing on the orange curve (i.e., the effective vaccinated population in Figure 2), and assuming that the initial time (t=0) for simulations was the week beginning 10^{th} December 2017.

The vaccine efficacy (**VE**) of influenza B viruses was obtained from CHP [24]. Because of insufficient data regarding VE for influenza A viruses in Hong Kong, such data was obtained from the Center for Disease Control and Prevention of the United States [25]. The overall VE was calculated using the subtypes VE and the ratio of subtypes infections data to overall infections data (D1 of Figure 1) from 5^{th} November 2017 to 5^{th} May 2018:

$$\mathrm{VE}_{Overall} = \sum^{i} \frac{\sum^{j} \mathrm{D1}_i}{\sum^{j} \mathrm{D1}_{total}} \cdot \mathrm{VE}_i, \quad i = \text{subtypes}, \quad j = \text{no. of weeks}. \tag{2}$$

Note that the influenza C virus was not included in the trivalent vaccine (see also Appendix A), and the effect of this virus on the VE calculation is negligible.

Subtype	Vaccine Efficacy	References
A(H1)	67%	[25]
A(H3)	25%	[25]
B	40%	[24]
Overall	45%	Calculated

Table 1: The efficacy of influenza vaccine against different viral subtypes.

In the following subsection, we start with a simple model in which we average the effect of all infection strains, and use this model to obtain an estimate of the average transmission and recovery rates. These rates will be used to approximate the corresponding rates for the more complex model 2 where different infection strains will be distinguished.

2.3. SVIR Model 1

2.3.1. Model Description

A SVIR model is proposed for the overall influenza epidemic in Hong Kong:

$$\frac{dS}{dt} = -\beta IS - r\big(1 - \frac{V_e}{A}\big), \tag{3a}$$
$$\frac{dV}{dt} = r\big(1 - \frac{V_e}{A}\big) - kIV, \quad \text{with} \quad k = \beta(1-w), \tag{3b}$$
$$\frac{dV_e}{dt} = r\big(1 - \frac{V_e}{A}\big), \tag{3c}$$
$$\frac{dI}{dt} = \beta IS + kIV - \gamma I, \tag{3d}$$
$$\frac{dR}{dt} = \gamma I. \tag{3e}$$

S : Susceptible	V : Vaccinated	I : Infected
R : Recovered	V_e : Effectively Vaccinated	

Table 2: Description of compartments of model 1.

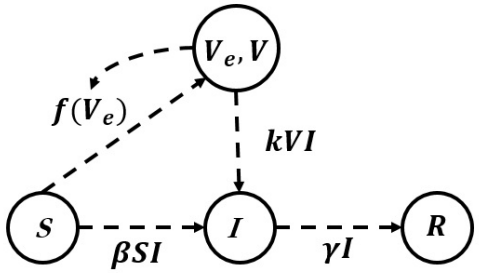

Figure 3: Transfer diagram for the SVIR model 1 given by equations (3). Here, $f(V_e) = r(1 - \frac{V_e}{A})$.

We divide the Hong Kong population into 4 compartments: Susceptible (S), Vaccinated (V), Infected (I), and Recovered (R). Since population in the vaccinated compartment V decreases because of infections, and thus cannot represent the true effectively vaccinated population (Figure 2), a separate sub-compartment V_e is introduced to show the effectively vaccinated population (although this is part of the compartment V). It is noted that both V and V_e

share the same initial value as both compartments are the same at the beginning. The model is explained graphically in Figure 3 and can be described as follows. Susceptible individuals are infected at a rate βSI and vaccinated at a rate $f(V_e)$ (see equation (1)). Since the vaccine is not perfect (i.e., VE$<$ 100%), vaccinated individuals are infected at a rate kVI, where k depends on the vaccine efficacy w and on the transmission rate β:

$$k = \beta(1 - w). \tag{4}$$

This equation has been adopted to show a "leaky" vaccine that offers partial protection to every vaccinated individual [26, 27, 28]. After being recovered from influenza at a rate γI, individuals are assumed to gain immunity and will not be infected again. The drawbacks of this assumption will be discussed in the "Discussion and Conclusion" section.

To simplify the calculations, since we assumed no net population growth rate and the total population of Hong Kong was 7.4 million during the study period, we rescaled the model such that the sum of the 4 compartments becomes equal to 1, i.e.,

$$\begin{aligned} S + V + I + R &= 7.4 \text{ million} \\ \Rightarrow \bar{S} + \bar{V} + \bar{I} + \bar{R} &= 1 \end{aligned} \tag{5}$$

with the bars being removed for simplicity.

2.3.2. Parameters Estimation

The weekly hospital admission data of different influenza subtypes (**DATA**) was obtained using the data sets D1 and D2 shown in Figure 1:

$$\text{DATA}_{subtype} = \text{D2} \cdot \frac{\text{D1}_{subtype}}{\text{D1}_{total}}, \tag{6}$$

and the result was plotted in Figure 4. The vertical blue dotted lines indicate the peak season (as determined in [18, 19]) and the vertical red dotted lines mark the two events related to the vaccination:

(1) Start of the vaccination schemes (week beginning 22^{nd} October 2017);

(2) Time when the first vaccination started to be effective (week beginning 5^{th} November 2017).

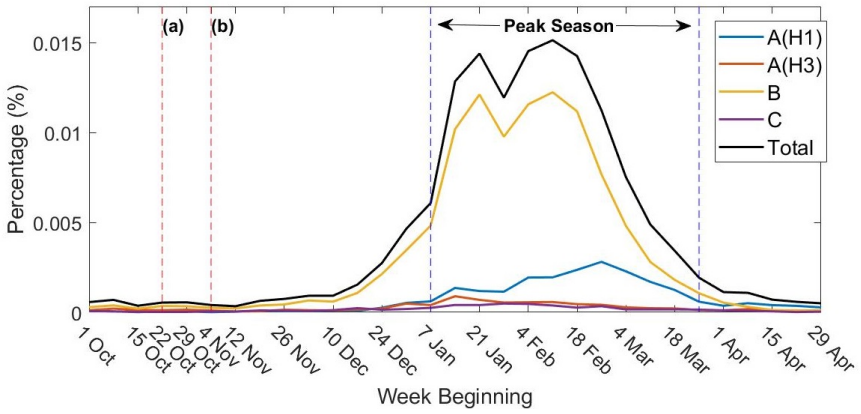

Figure 4: Weekly hospital admission data of different influenza subtypes (**DATA**) from 1^{st} October 2017 to 5^{th} May 2018. "(a)" indicates the start of vaccination schemes and "(b)" indicates the week when first vaccination started to be effective. The peak season is bounded by the purple dotted lines.

As it is impossible to obtain the actual number of infections in Hong Kong, we need to estimate the actual number of infections using the available data. We assume that the actual number of weekly infections is directly proportional to the weekly hospital admissions due to influenza (DATA) (see equation (6) and Figure 4), with the proportionality ratio α. Since we also assumed that 15% of Hong Kong population was infected by influenza over the peak season (see the assumption in Section 2.1), we transform DATA within the peak season into a cumulative distribution (C) and use the following equation to estimate α:

$$\alpha = \frac{\text{HK population} \cdot \%\text{ of infection over the season}}{C_{end\ of\ season}} \Rightarrow \tag{7}$$

$$\alpha = \frac{7.4 \text{ million} \cdot 0.15}{0.0012} \approx 127.$$

To estimate the actual weekly number of infections of different influenza subtypes (**DATA2**), we then multiply the weekly hospital admission data (DATA)

by the proportionality ratio α, as follows:

$$\text{DATA2 (weekly)} = \alpha \cdot \text{DATA (weekly)}. \tag{8}$$

DATA2 is plotted in Figure 5. In Figure 6 we plot the infected compartment of model 1 against DATA2. The approach taken in this figure (i.e. fit the infected compartment to the observed data) is different from the classical approach (where one integrates γI and then matches it to weekly data [29, 30]). The red squares in the figure show the total infection data from DATA2 and its cumulative distribution over the study period. The model is fitted to the data by least squares method to determine the parameters. The initial value $I(0) = 0.0012$ is obtained from DATA2, $R(0) = 0$ by assumption, $V(0), V_e(0) \approx 0.0565$ (with V_0 from Figure 2), and $S(0) = 0.9424$ is calculated by equation (5).

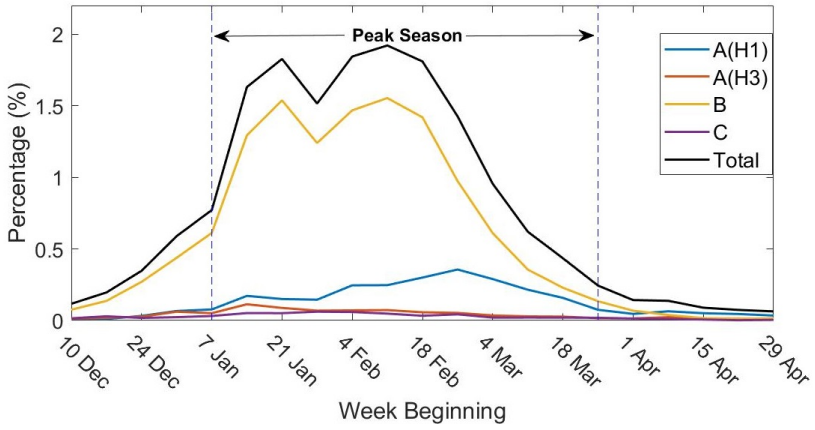

Figure 5: Weekly infection data of different influenza subtypes (**DATA2**) over the study period. Influenza peak season is bounded by the dotted lines.

From the fitting in Figure 6, we obtain the average transmission rate and the recovery rate: $\beta \approx 2.7516$ and $\gamma \approx 2.1272$. We then use the following relationship between the recovery rate γ and the recovery period T,

$$T\ (day) = \frac{1}{\gamma\ (week^{-1})} \cdot 7, \quad \text{(where 7 days = 1 week)} \tag{9}$$

to approximate the recovery period to $T \approx 3.29$ days. Note that this period is slightly shorter than the recovery period for different past seasonal influenza

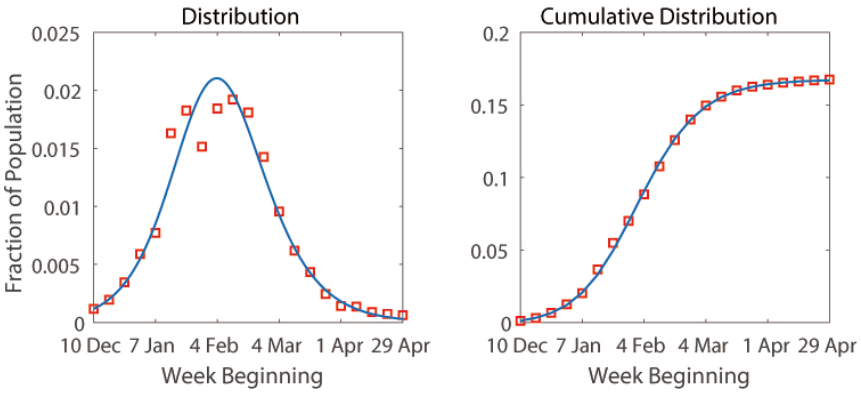

Figure 6: Infected compartment of model 1 and its cumulative distribution over study period. Red squares indicate the weekly data and the blue curves are the fitted numerical solution of model 1.

epidemics (for example, [31] approximated the recovery period to 4.1 days, while [32] used a recovery period of 3.8 days). The parameters are listed in Table 3 and the dynamics of the SVIR model is plotted in Figure 7. The details of the linear stability analysis of model 1 are discussed in Appendix B. We will use the approximated values of β and γ in the next section, where we will focus on infections with different influenza subtypes.

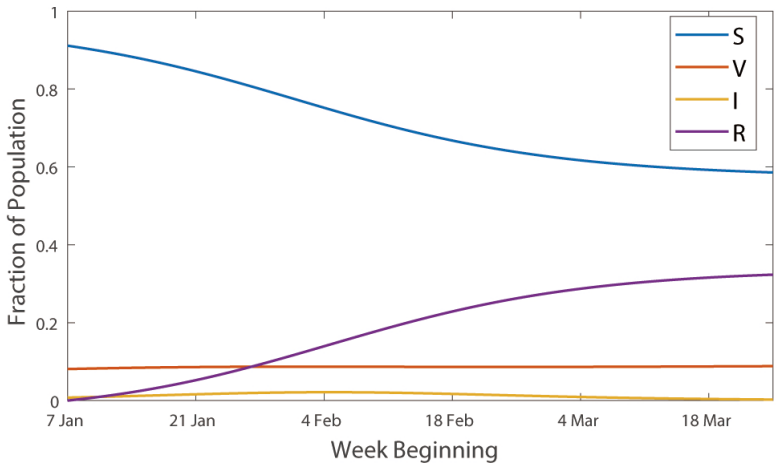

Figure 7: Dynamics of SVIR model 1 over the study period.

Symbol	Description	Value	References
α	Infected ratio	127	Calculated
S(0)	Initial value of compartment S	0.9424	Calculated
V(0)	Initial value of compartment V	0.0565	Figure 2
$V_e(0)$	Initial value of compartment V_e	0.0565	Figure 2
I(0)	Initial value of compartment I	0.0012	DATA2
R(0)	Initial value of compartment R	0	Assumed
r	Growth rate of effectively vaccinated population	0.0155	Fitted
A	Maximum of effectively vaccinated population	0.1155	Fitted
β	Transmission rate of susceptible individuals (1/week)	2.7516	Fitted
γ	Recovery rate (1/week)	2.1272	Fitted
w	Overall vaccine efficacy	0.45	Table 1
k	Infection rate (1/week) of vaccinated individuals, calculated using the formula $k = \beta(1-w)$	1.5134	Calculated
T	Recovery period (days)	3.29	Calculated
R_0	Basic reproductive ratio	1.2935	Calculated
R_{0x}	Effective reproductive ratio	1.2607	Calculated

Table 3: Parameters used in model 1, with their descriptions and approximated values.

2.4. SVIR Model 2

2.4.1. Model Description

Next we propose another SVIR model (relatively similar to model 1) which distinguishes between the infection generated by different influenza subtypes. For indices i = A(H1), A(H3), B, corresponding to the influenza A(H1),A(H3) and B viruses, we have

$$\frac{dS}{dt} = -\sum_{i=1}^{3} \beta_i I_i S - r(1 - \frac{V_e}{A}) \tag{10a}$$

$$\frac{dV}{dt} = r(1 - \frac{V_e}{A}) - \sum_{i=1}^{3} k_i I_i V, \qquad k_i = \beta_i \cdot (1 - w_i) \tag{10b}$$

$$\frac{dI_i}{dt} = \beta_i I_i S + k_i I_i V - \gamma_i I_i \tag{10c}$$

$$\frac{dR}{dt} = \sum_{i=1}^{3} \gamma_i I_i \tag{10d}$$

$$\frac{dV_e}{dt} = r(1 - \frac{V_e}{A}) \tag{10e}$$

S : Susceptible	V : Vaccinated	$I_{A(H1)}$: Type A(H1) Infected
$I_{A(H3)}$: Type A(H3) Infected	I_B : Type B Infected	R : Recovered
V_e : Effectively vaccinated		

Table 4: Description of compartments of model 2.

Similar to model 1, we divide the Hong Kong population into 6 compartments: Susceptible (S), Vaccinated (V), type A(H1) Infected ($I_{A(H1)}$), type A(H3) Infected ($I_{A(H3)}$), type B Infected (I_B), and Recovered (R). As in model 1, in addition to the compartment V, we consider the sub-compartment V_e describing the effectively vaccinated population. The model is explained graphically in Figure 8 and can be described as follows. Susceptible individuals are infected by influenza subtypes i at a rate $\beta_i SI_i$ and vaccinated at a rate $f(V_e)$ (see equation (1)). Since the vaccine is not fully protective on each subtype

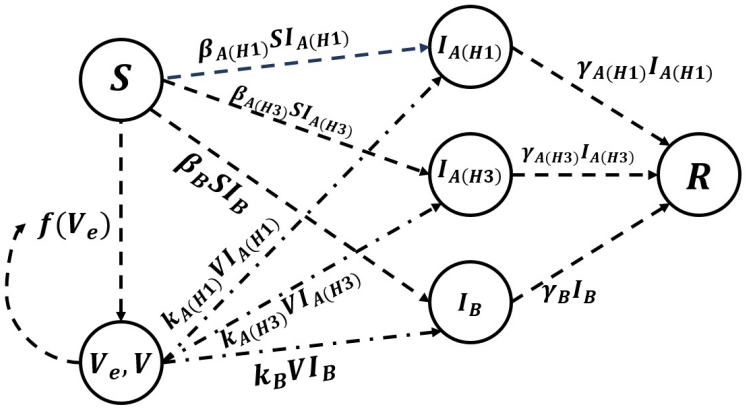

Figure 8: Transfer diagram of SVIR model 2. $f(V_e) = r(1 - \frac{V_e}{A})$

($w_i < 100\%$), vaccinated individuals are infected at a rate $k_i V I_i$ where k_i depends on the vaccine efficacy w_i and on the transmission rate β_i:

$$k_i = \beta_i(1 - w_i), \text{ where } i = A(H1), A(H3), B. \tag{11}$$

This equation has been adopted to show a "leaky" vaccine that offers partial protection to every vaccinated individual [26, 27, 28]. After being recovered from influenza at a rate $\gamma_i I_i$, individuals are moved to the recovered compartment R. For simplicity, we assume no cross-infections between viruses, and individuals who were once infected obtain immunity and will not be infected again by any other influenza viruses. The drawbacks of this assumption will be discussed in the "Discussion and Conclusion" section.

As we assumed no net population growth rate and the total population of Hong Kong was 7.4 million during the study period, the model is re-scaled such that the sum of the 6 compartments equals to 1, i.e.,

$$\begin{aligned} &S + V + I_{A(H1)} + I_{A(H3)} + I_B + R = 7.4 \text{ million} \\ &\Rightarrow \bar{S} + \bar{V} + \bar{I_{A(H1)}} + \bar{I_{A(H3)}} + \bar{I_B} + \bar{R} = 1 \end{aligned} \tag{12}$$

with the bars being removed for simplicity.

2.4.2. Parameters Estimation

DATA2 are used for the fitting in model 2 (Figure 5). The initial values of infected compartments, $I_{A(H1)}$, $I_{A(H3)}$, I_B are obtained from DATA2 (please see Table 6). Similar to model 1, we choose $R(0) = 0$, $V(0), V_e(0) \approx 0.0565$ (V_0 from Figure 2), while $S(0) = 0.9425$ is calculated by equation (12).

Since more parameters are involved in this model, we combine the bootstrap method with the least squares method to estimate the parameters and show the fitting accuracy. The bootstrap method is a numerical techniques for statistical inference, which is used to show the accuracy of the estimators for the unknown parameters [9]. In order to use this method, we re-sample DATA2 to be Poisson distributed at a fixed time, with mean equal to the original data. Each set of generated samples is used to simulate a similar influenza season and least squares method is used to determine the parameters in each simulation; this procedure is repeated 2000 times. Figure 9 and Table 5 show the distributions and results of bootstrapping estimation of the parameters. As A(H3) viral infections were insignificant compared to other 2 subtypes, we assumed the recovery rate of A(H3) viruses to be the average recovery rate estimated in Table 3 (to facilitate the MATLAB estimator to converge to a set of parameter values).

Symbol	Fitted value	Mean	S.D.	95% C.I	
$\beta_{A(H1)}$	1.9528	1.9400	0.1160	[1.6070	2.0911]
$\beta_{A(H3)}$	2.5911	2.5911	0.0068	[2.5807	2.6018]
β_B	3.0911	3.0953	0.0229	[3.0698	3.1702]
$\gamma_{A(H1)}$	1.3581	1.3471	0.0963	[1.0693	1.4699]
γ_B	2.4138	2.4179	0.0209	[2.3983	2.4928]

Table 5: Bootstrapping results.

The infected compartments of the model are shown in Figure 10. The fitted value of each parameter in Table 5 is taken from the mean value of the middle 10% of the histograms in Figure 9. The recovery period T can then be calculated using equation (9). The parameters are listed in Table 6 and 7, and the dynamics

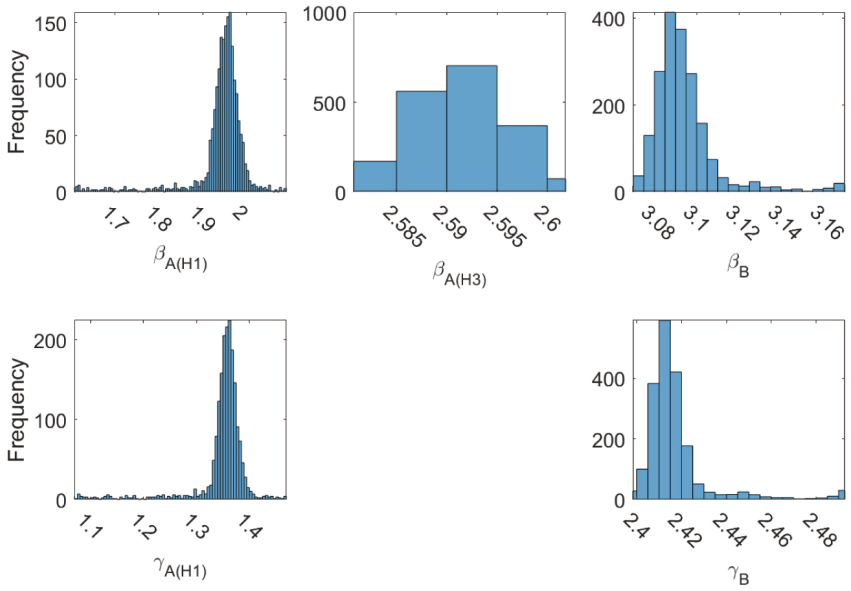

Figure 9: Histogram results of the bootstrap method.

of the SVIR model is plotted in Figure 11a. In order to show the dynamics of the infection compartments clearly, their dynamics are plotted in Figure 11b with an appropriate scale.

The infected compartments of model 2 (10) are shown in Figure 10. The fitted value of each parameter in Table 5 is taken from the mean value of the middle 10% of the histograms in Figure 9. The recovery period T can then be calculated using equation (9). The parameters are listed in Table 6 and 7, and the dynamics of the SVIR model is plotted in Figure 11a. In order to show the dynamics of the infection compartments more clearly, their dynamics are plotted in Figure 11b on an appropriate vertical scale.

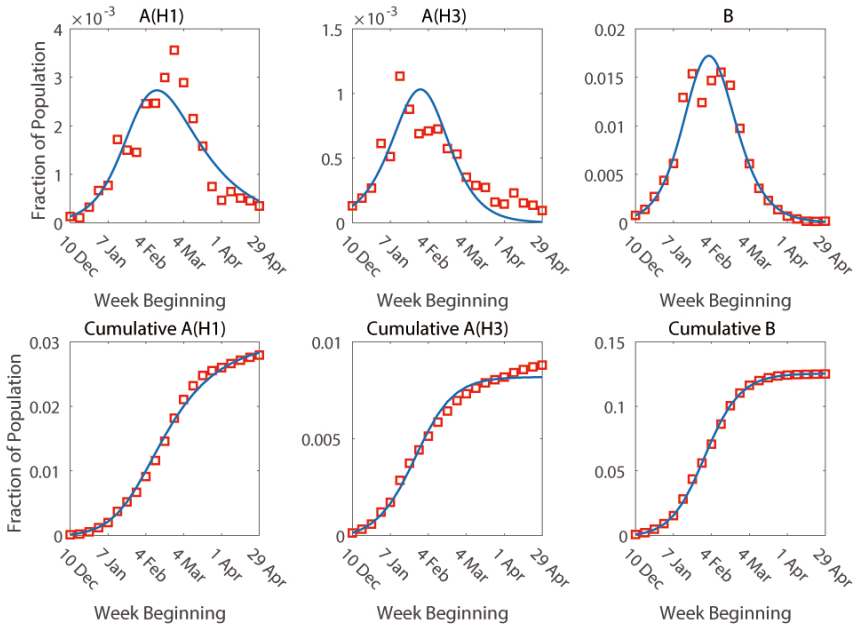

Figure 10: Infected compartments of model 2 and their cumulative distributions. (Upper row) Time-evolution of the infected compartments of model 2, and (Lower row) their cumulative distributions. Red squares indicate the weekly data and the blue curves are the fitted numerical solution of model 2.

As observed in Figure 10, the estimation of influenza A(H1) and B infections are satisfactory, but the fitted curve for influenza A(H3) viruses is below the actual data towards the end of the season. Since the infected compartment of the SVIR model (10) will approach a zero steady state as time goes by (as it will be discussed later in this section), the difference between the zero steady states and the real data will be significant if the data remained at a low nonzero level throughout the period of interest. As the A(H3) viral infections remained at a significant low level that was on a comparable scale to the number of influenza infections in the non-peak season (see Figure 1), this difference is significant, and cannot be eliminated. However, since the B viral infections occurred in greater numbers (see Figure 1), this difference between simulated curve and actual data is negligible.

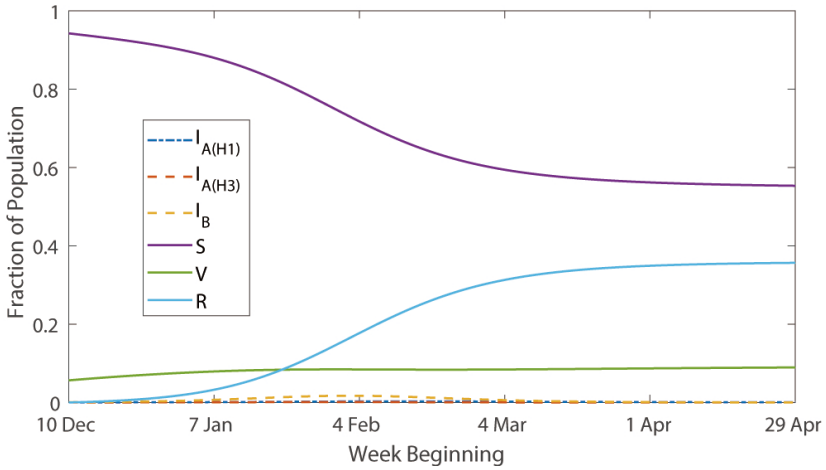

(a) All compartments

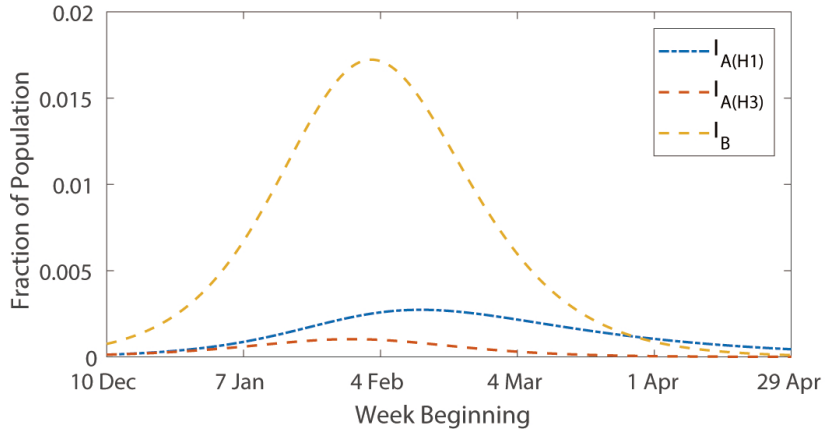

(b) Infected compartments

Figure 11: Dynamics of SVIR model 2 over study period.

2.4.3. Steady States and Their Stability

The details of the linear stability analysis for model 2 are discussed in Appendix C. From this analysis, R_0 and R_{0x} of each virus subtype are defined as follows (see equation (24) and (25) in Appendix C):

$$R_{0i} = \frac{\beta_i}{\gamma_i}, \quad i = A(H1), A(H3), B, \tag{13}$$

Symbol	Description	Value	References
α	Infected ratio	127	Calculated
S(0)	Initial value of compartment S	0.9425	Calculated
V(0)	Initial value of compartment V	0.0565	Figure 2
$V_e(0)$	Initial value of compartment V_e	0.0565	Figure 2
$I_{A(H1)}(0)$	Initial value of compartment $I_{A(H1)}$	$1.3062e^{-4}$	DATA2
$I_{A(H3)}(0)$	Initial value of compartment $I_{A(H3)}$	$1.3062e^{-4}$	DATA2
$I_B(0)$	Initial value of compartment $I_B(0)$	$7.5470e^{-4}$	DATA2
R(0)	Initial value of compartment R	0	Assumed
r	Growth rate of effectively vaccinated population	0.0155	Fitted
A	Maximum of effectively vaccinated population	0.1155	Fitted
$\beta_{A(H1)}$	Transmission rate of A(H1) viruses of susceptible individuals (1/week)	1.9528	Fitted
$\beta_{A(H3)}$	Transmission rate of A(H3) viruses of susceptible individuals (1/week)	2.5911	Fitted
β_B	Transmission rate of B viruses of susceptible individuals (1/week)	3.0911	Fitted
$\gamma_{A(H1)}$	Recovery rate of A(H1) viruses (1/week)	1.3581	Fitted
$\gamma_{A(H3)}$	Recovery rate of A(H3) viruses (1/week)	2.1272	Table 3
γ_B	Recovery rate of B viruses (1/week)	2.4138	Fitted
$w_{A(H1)}$	Vaccine efficacy of A(H1) viruses	0.67	Table 1
$w_{A(H3)}$	Vaccine efficacy of A(H3) viruses	0.25	Table 1
w_B	Vaccine efficacy of B viruses	0.4	Table 1
$T_{A(H1)}$	Recovery period of A(H1) viruses (days)	5.15	Calculated
$T_{A(H3)}$	Recovery period of A(H3) viruses (days)	3.29	Calculated
T_B	Recovery period of B viruses (days)	2.90	Calculated

Table 6: Parameters used in model 2, with their descriptions and approximated values.

Symbol	Description	Value	References
$k_{A(H1)}$	Transmission rate of A(H1) viruses of vaccinated individuals (1/week)	0.6444	Calculated
$k_{A(H3)}$	Transmission rate of A(H3) viruses of vaccinated individuals (1/week)	1.9433	Calculated
k_B	Transmission rate of B viruses of vaccinated individuals (1/week)	1.8547	Calculated
$R_{0A(H1)}$	Basic reproductive ratio of A(H1) viruses	1.4378	Calculated
$R_{0A(H3)}$	Basic reproductive ratio of A(H3) viruses	1.2181	Calculated
R_{0B}	Basic reproductive ratio of B viruses	1.2806	Calculated
$R_{0xA(H1)}$	Effective reproductive ratio of A(H1) viruses	1.3834	Calculated
$R_{0xA(H3)}$	Effective reproductive ratio of A(H3) viruses	1.2009	Calculated
R_{0xB}	Effective reproductive ratio of B viruses	1.2517	Calculated

Table 7: Parameters used in model 2, with their descriptions and approximated values (Continue).

$$R_{0xi} = \frac{\beta_i}{\gamma_i}(1 - w_i V_0), \quad i = A(H1), A(H3), B, \quad V_0 = V(0). \tag{14}$$

Using the parameter values from Table 6, we can obtain both reproductive ratios (R_{0i} and R_{0xi}) for each virus subtype (see their values in Table 7). Since R_{0x} of all virus subtypes are greater than one over the whole study period, infections from all subtypes continued to spread.

The steady states of the model 2 are

$$(S, V, V_e, I_{A(H1)}, I_{A(H3)}, I_B, R) = (1 - V^* - R^*, V^*, A, 0, 0, 0, R^*),$$

where $0 \leq V^*, R^*$, $V^* + R^* \leq 1$, $V^* \leq A$. We consider $R(0) = R^*$ and $V(0) = V^*$ to observe the stability of the steady states at the beginning of the influenza season. By simple calculation we can find the eigenvalues of the Jacobian matrix associated with the system (10) (see also equation (26) in Appendix C):

$$\lambda_i = \beta_i\big(1 - w_i V(0) - R(0)\big) - \gamma_i, \quad \text{where} \quad i = A(H1), A(H3), B. \tag{15}$$

Hence if the inequality

$$\beta_i\big(1 - w_i V(0) - R(0)\big) - \gamma_i > 0$$

is satisfied for any subtype i, the steady states are unstable. We then consider λ to be the largest λ_i (i.e., $\lambda = \max \lambda_i$); then $\lambda < 0$ indicates that the steady state is stable (since $\max \lambda_i < 0 \Rightarrow \lambda_i < 0,\ \forall\ i$).

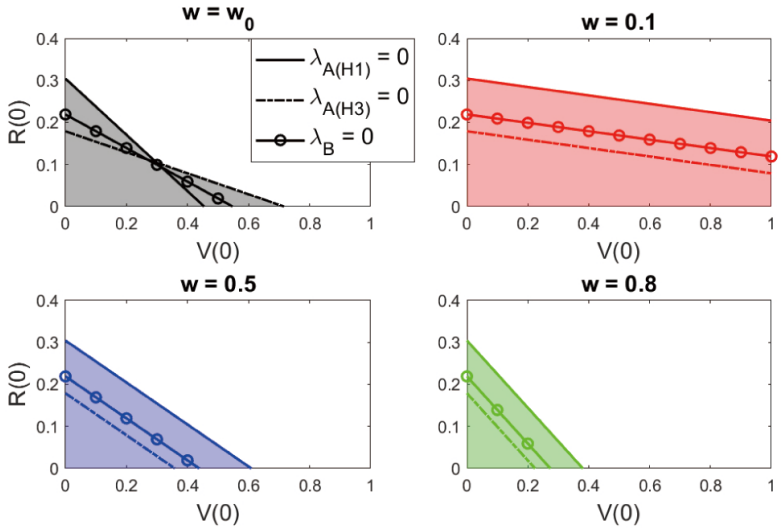

Figure 12: The dynamics of the determining eigenvalues λ_j in the $(V^*,\ R^*)$=$(V(0),\ R(0))$ space, for different vaccine efficacies $w = w_{A(H1)} = w_{A(H3)} = w_B$ and influenza subtypes j. The baseline vector $w_0 = (w_{A(H1)}, w_{A(H3)}, w_B) = (0.62, 0.25, 0.4)$ is obtained from Table 6. In each sub-figure the solid, dashed-dotted and dashed lines represent $\lambda_j = 0$, where $j = A(H1), A(H3)$ and B respectively (see equation (26) in Appendix C). The shaded areas represent the values of $V(0)$ and $R(0)$ where $\max(\lambda_j) > 0$.

Figure 12 shows the changes in the stability of the steady state (corresponding to the changes in the sign of λ) for different vaccine efficacies $w = w_{A(H1)} = w_{A(H3)} = w_B$. If we now focus on the case $R(0) = V(0) = 0$ at the beginning of the season, we observe that this disease-free equilibrium is always unstable, i.e., a single infection case will cause the spread of the influenza. As the vaccine efficacies w increase ($w = 0.1 \to 0.5 \to 0.8$), the level of the initial vaccinated

population $V(0)$ that can ensure stable steady states does decrease (see how the unshaded region in Figure 12 moves towards left). We also observe that when $w = 0.1$ and $R(0) \approx 0$, the disease-free equilibrium is unstable even if the whole Hong Kong population are vaccinated ($V(0) = 1$).

3. Numerical Simulations

In this section, we investigate the effects of different vaccination strategies applied to model 2 (given by equations (10)), where we change the initial vaccinated population V(0) and the vaccine efficacy w_i of each influenza subtype. For each strategy, all parameters are assumed to be the same as in Table 6 and Table 7 except for the parameter that we are changing.

3.1. Initial Vaccinated Population

We assume that the initial vaccinated population is constant and no further vaccination occurs, i.e., $A = V(0),\ 0 < V(0) < 1,\quad r = 0$. Then equation (10b) becomes

$$\frac{dV}{dt} = -\sum_{i=1}^{3} k_i I_i V. \tag{16}$$

We observe in Figure 13 that by increasing $V(0)$, the influenza epidemic becomes smaller and smaller. We also observe that, for different influenza subtypes, different V(0) are required to clear out the infections spread from the beginning.

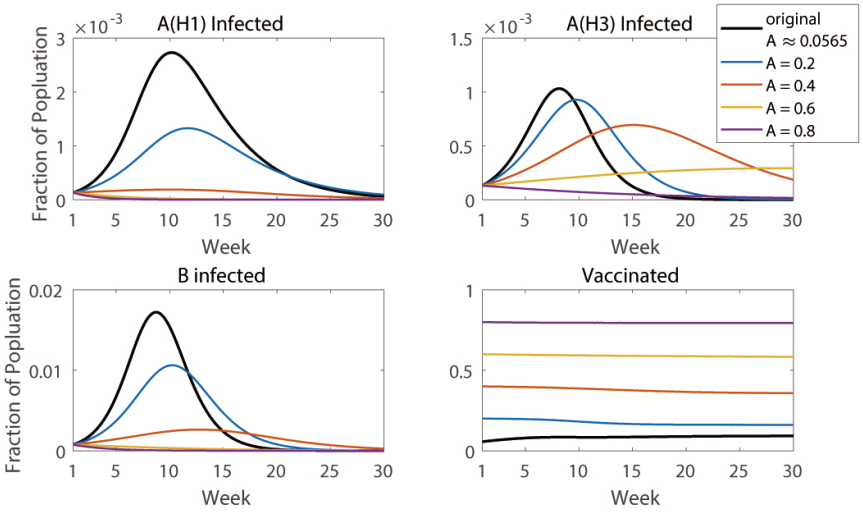

Figure 13: The dynamics of SVIR model 2, for different initial vaccination population. $A = V(0) = V_e(0)$. The baseline $A = 0.0565$ is obtained from $V(0)$ in Table 6.

3.2. No Vaccination

In Figure 14 we consider the case when no vaccine is available in Hong Kong and thus no one is vaccinated during the influenza season. Without vaccine protection (i.e., $V(t) = 0, \quad \forall t \geq 0$), it is obvious that the total number of infections will be higher. Because of the small A(H3) infected population and the low VE of A(H3) viruses, the vaccination against A(H3) has an insignificant effect.

To see more clearly why these results hold, let us return to system (10) where we add the susceptible and vaccinated compartments:

$$\frac{d(S+V)}{dT} = -\sum_{i=1}^{3} \beta_i I_i \Big(S + (1-w_i)V \Big)$$

$$\Rightarrow \frac{d(S+V)}{dT} = -\sum_{i=1}^{3} \beta_i I_i (S+V), \text{ if } w_i = 0 \ \forall i.$$

Relabelling $S + V = \tilde{S}$, we have

$$\tilde{S} = -\sum_{i=1}^{3} \beta_i I_i \tilde{S}. \tag{17}$$

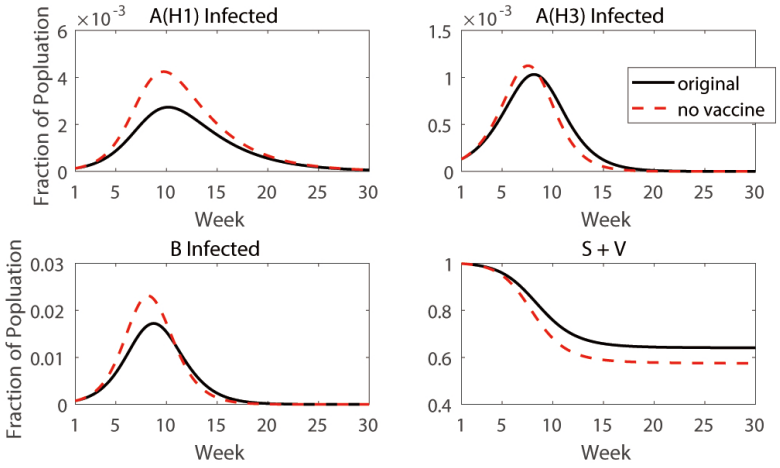

Figure 14: The dynamics of SVIR model 2 without any vaccination. Bottom right panel shows the summation of susceptible and vaccinated compartments.

Thus, if the vaccine is not effective at all ($w_i = 0, \forall i$), it will result in the same situation as when no one has been vaccinated.

3.3. Vaccine Efficacy

In general, the influenza vaccines can have low efficacies (i.e., $w_i < 1$) [33]. However, vaccine efficacy could be increased by increasing the vaccine immunogenicity or the breadth of the immune response, which can be done, for example, by incorporating adjuvants (that stimulate the antiviral immune response, and thus can increase vaccine effectiveness against all strains), or by injecting higher amounts of virus antigens (and thus increasing vaccine effectiveness against the particular virus strain injected at higher levels) [34, 35].

Mathematically, we can investigate the possible increase in vaccine efficacy (VE) by considering the following two cases/methods:

1. Change one VE (i.e. w_i for $i = A(H1), A(H3)$ or B) while keeping other two VE unchanged (see Figure 15).
2. Change all VE together to one fixed value $w = w_{A(H1)} = w_{A(H3)} = w_B$ (see Figure 16).

Note that changing the vaccine efficacies w_i leads to changes in the infection rates k_i for the vaccinated individuals; see equation (11).

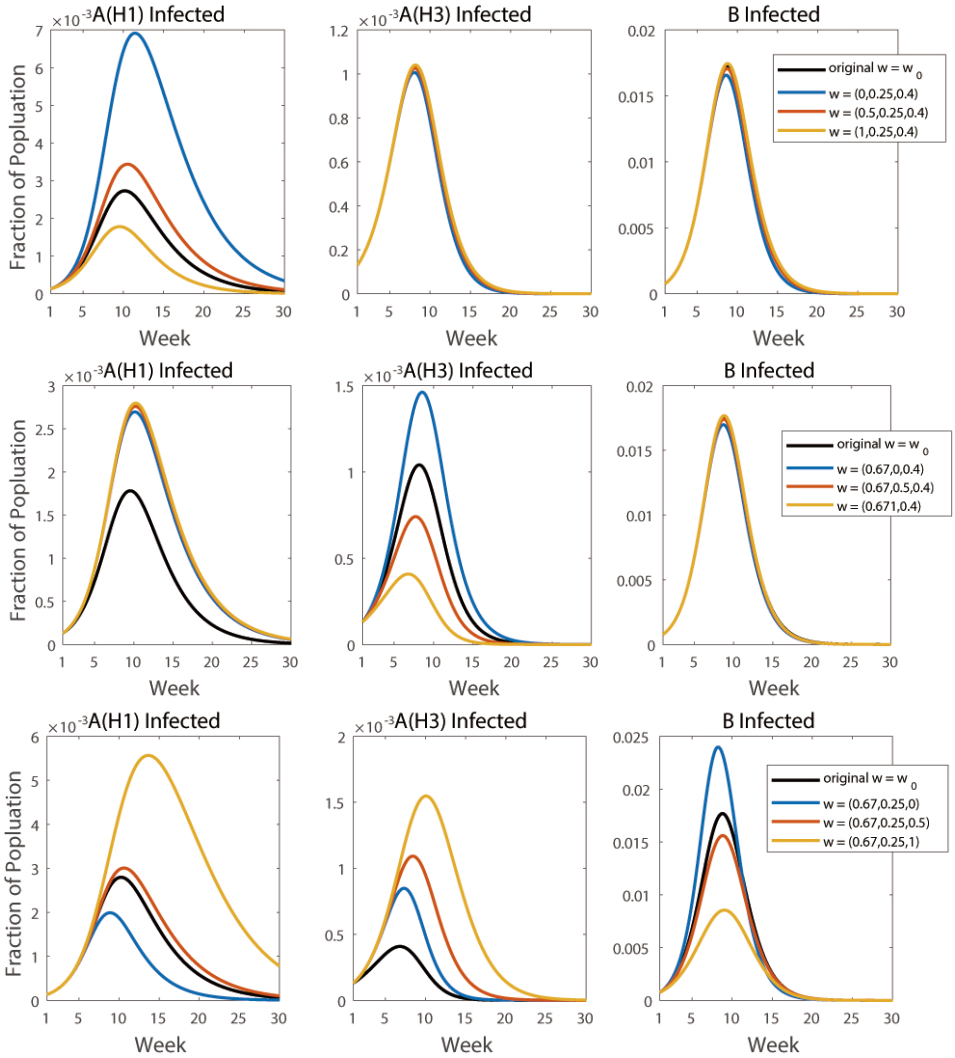

Figure 15: The dynamics of SVIR model 2, when the vaccine efficacy of each influenza subtype is being changed separately. In the legend, we denoted by w the efficacy vector $w = (w_{A(H1)}, w_{A(H3)}, w_B)$. The baseline vector $w_0 = (0.67, 0.25, 0.4)$ contains the baseline efficacy parameters identified for model 2 (see Table 6). (Top row) $w_{A(H1)}$ is being changed. (Middle row) $w_{A(H3)}$ is being changed. (Bottom row) w_B is being changed.

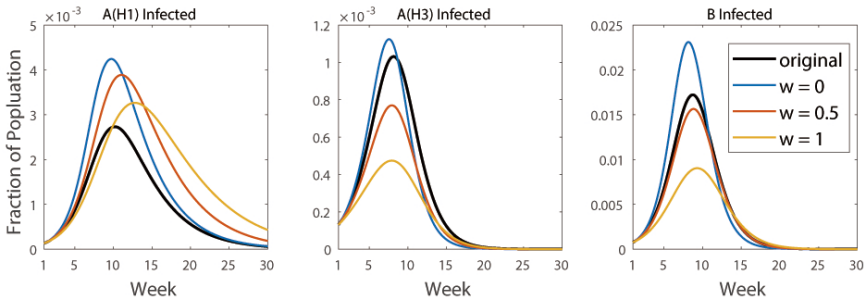

Figure 16: The dynamics of SVIR model 2, when the vaccine efficacies for the influenza subtypes are being changed together to one fixed scalar value $w = w_{A(H1)} = w_{A(H3)} = w_B$. The baseline (i.e., original) vector $w_0 = (0.67, 0.25, 0.4)$ is obtained from Table 6.

For method 1 (see Figure 15), we observe that when w_i for subtype i is higher than its baseline value in the vector $(w_{A(H1)}, w_{A(H3)}, w_B) = (0.67, 0.25, 0.4)$, the results always show smaller epidemics of that particular subtype. However, the increase of any VE will lead to an increase in the number of infections for the other two subtypes. Since the infections with one subtype decreased, it lead to more susceptibles that can be infected by the other two virus subtypes. Also, since the decrease of B infections released many more susceptibles (as B strain was the dominant virus), the number of infections with other two subtypes increased significantly.

A similar trend can be observed for method 2 (see Figure 16). Although the number of infections with A(H3) and B viruses decreased with the increase in the VEs (see the middle and right panels in Figure 16), a more severe epidemic was caused by the A(H1) virus (see the left panel). This could be the result of the higher reproductive ratio of A(H1) (see Table 7, where $R_{0xA(H1)}$ is the highest among the three subtypes), and that the stop of the spread of B infections (which is the dominant virus in that season) will lead to more susceptible for the spread of A(H1) infections. We will return to this discussion in Section 3.5.

In addition, we observe that the perfect vaccine efficacy cannot stop the spread of influenza infections (see the yellow curves for $w = 1$ in Figure 16). We hypothesise that the current level of vaccination coverage in Hong Kong is not

enough to stop the spread of the infection. We will return to this discussion in Section 3.6.

3.4. Partially Perfect Vaccine

We observe from Section 3.3 that A(H1) viral infections will become severe if a perfect vaccine is introduced. In this Section we carry out simulations to investigate if there are any possible VE combinations that will result in a smaller epidemic.

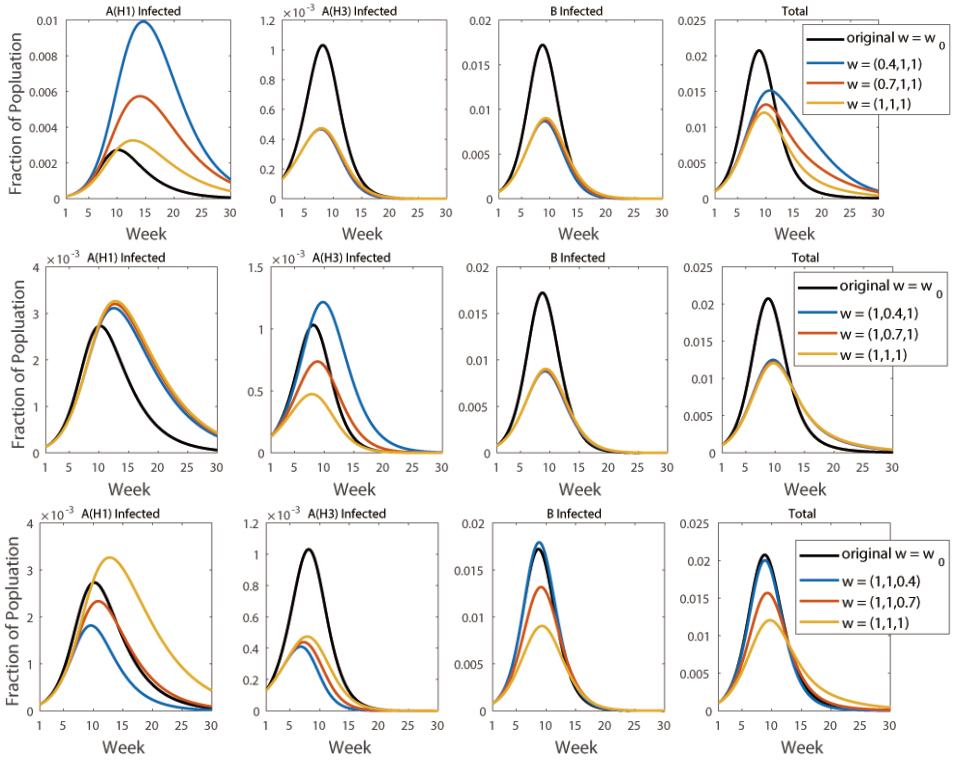

Figure 17: The dynamics of SVIR model 2, when we vary the vaccine efficacy against one subtype and assume 100% efficacies against the other two subtypes. The efficacy vector is $w = (w_{A(H1)}, w_{A(H3)}, w_B)$. (Top row) The effect of varying $w_{A(H1)}$. (Middle row) The effect of varying $w_{A(H3)}$. (Bottom row) The effect of varying w_B.

First, we define a "partially perfect vaccine" to be a vaccine with 100% VE

on any two influenza subtypes and less than 100% VE on the third subtype. Second, we assume that the vaccination coverage is as described in Figure 2. Moreover, we assume 100% VE on any 2 influenza subtypes, with the remaining subtype VE varying from 40% to 100%. The simulation results are plotted in Figure 17. We can easily observe that an increase in one VE will always lead to an increase in the number of A(H1) infections. A possible explanation for this increase is discussed in more detail in Section 3.5. However, despite the increase in the A(H1) infections, we note that the total number of infections is decreasing with increased vaccine efficacy w_i, and the perfect vaccine (obtained for $w_i = 1,\ \forall i$) will result in the smallest epidemic; see the fourth column in Figure 17.

3.5. Parameter sensitivity test on changes in w_i

Sensitivity of R_{0xi}

A puzzling result in Sections 3.3 and 3.4 was that when VE was high (e.g., 100%), the number of A(H1) infections still increased. To obtain a better understanding of the mechanisms behind this increase, here we focus on the effective reproductive ratio for each influenza subtype R_{0xi} (as given by equation (14)):

$$R_{0xi} = \frac{\beta_i}{\gamma_i}\big(1 - w_i V_0\big), \quad i = A(H1), A(H3), B.$$

In Figure 18 we show the changes in R_{0xi} as functions of w_i, where the rest of the parameter values are fixed as in Table 6.

Since the vaccinated population increases as time passes (see Figure 2), by mid February ($\approx$ week 10) $R_{0xA(H1)}$ should still be the highest among the effective reproductive ratios for the three influenza subtypes (where R_{0xi} are calculated based not on the original V_0 but on the V on $\approx$ week 10). Moreover, as the efficacies increase towards $w_i = 1$, $R_{0xA(H3)}$ and R_{0xB} are decaying towards the value 1.1 while $R_{0xA(H1)}$ is still well above the value 1.3 (see Figure 18), and thus we still expect a fast increase in the A(H1) cases. In addition, since the number of B infections (the highest among the three subtypes) has been reduced, it leaves more susceptible for the A(H1) infections. When these two

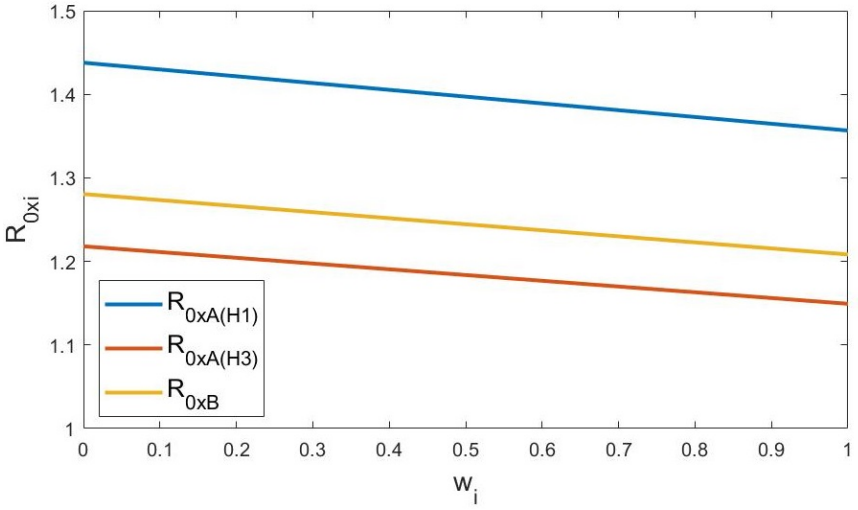

Figure 18: Plot of effective reproductive ratio for each influenza subtype i (R_{0xi}) against vaccine efficacy (w_i). R_{0x} is calculated using equation (14). The parameters used in the equation are obtained from Table 6.

factors co-exist (i.e., higher $R_{0x(AH1)}$ and more susceptibles), the number of A(H1) infections increases to values larger than the original/baseline ones (as observed in Figures 15-17). This explanation can account also for the small increase in the A(H3) infections shown in Figure 17 bottom row as we increase $w_B = 0.4 \to 0.7 \to 1$ (since $R_{0xA(H3)}$ is still relatively high, and more susceptible are in the environment due to the increase in the efficacy of B vaccine).

Sensitivity of attack rate

Next, we perform a Partial Rank Correlation Coefficient (PRCC) sensitivity analysis [36] with the help of R software (function *pcc* of the package *sensitivity*). To this end, we simulate the impact of three vaccine efficacies $(w_{A(H1)}, w_{A(H3)}, w_B)$ on the attack rate (cumulated proportion) of influenza virus strains A(H1), A(H3) and B (see Figure 19). For the sampling, we sample randomly 1000 times each of the parameters $w_{A(H1)}, w_{A(H3)}, w_B$ from the range [0,1]. Then, we calculate the PRCC of cumulative cases of influenza virus strains

A(H1), A(H3) and B against the efficacy parameters $w_{A(H1)}$, $w_{A(H3)}$ and w_B. Note that the PRCC values that are closer to +1 or -1 indicate that the sampling parameter has a greater influence on the outcome measure [36]. Moreover, a negative sign indicates that the sampling parameter is inversely proportional to the outcome measure, while a positive sign indicates that the parameter is directly proportional to the outcome [36]. In Figure 19 we observe that the attack rate of A(H1) is negatively correlated to its own vaccine efficacy $w_{A(H1)}$, but positively correlated to the other vaccine efficacies, $w_{A(H3)}$ and w_B. This means that a reduction in $w_{A(H1)}$ will increase the fraction of A(H1)-infected, while a reduction in w_B will decrease the fraction of A(H1)-infected – as seen in Figure 15 first column (note that the PRCC value of $w_{A(H3)}$ corresponding to the A(H1) attack rate is less than 0.5, suggesting a weak influence on this attack rate). Similar results are shown for the other two influenza strains.

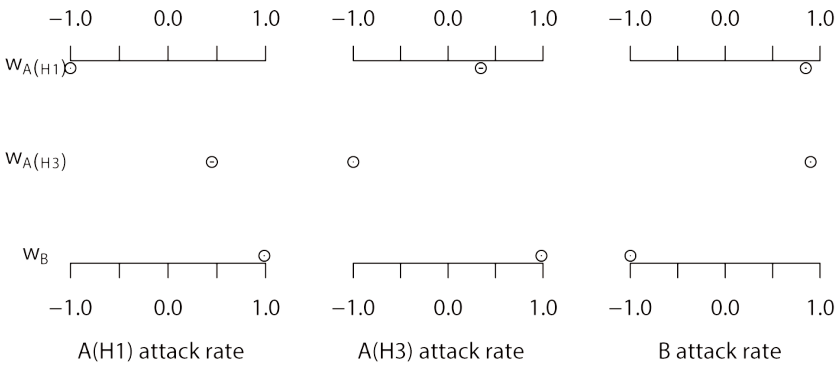

Figure 19: Attack rate of different influenza viruses (A(H1), A(H3), B) against different vaccine efficacies ($w_{A(H1)}, w_{A(H3)}, w_B$) tested in PRCC of R package *sensitivity*. We simulate for 25 weeks with a step size 1/7 week (1 day) and 1000 random samples of ($w_{A(H1)}, w_{A(H3)}, w_B$).

3.6. Critical Vaccination Threshold

The equation for the critical vaccination threshold V_c, when considering the vaccine efficacy w, is [37]:

$$V_c = \left(1 - \frac{1}{R_0}\right) \cdot \frac{1}{w}, \tag{18}$$

where R_0 is the basic reproductive ratio. The formulation of this equation is discussed in Appendix D. By substituting the parameter values from Table 6 into (18) we can obtain the thresholds of different influenza subtypes which are listed in Table 8. Noted here that all V_c calculated with 100% VE are higher than the original maximum vaccinated population ($\sim$ 11.6%). This could explain the result in Section 3.3 where the lack of vaccination coverage resulted in an epidemic even when the vaccine was perfect.

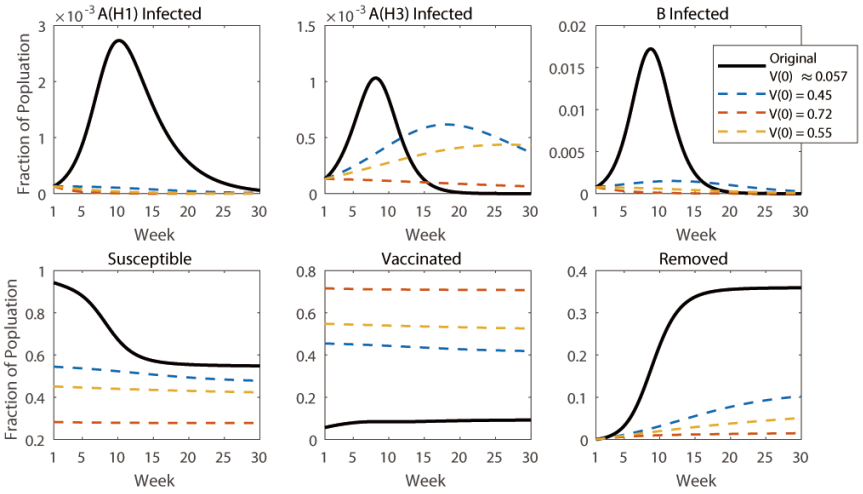

(a) $(w_{A(H1)}, w_{A(H3)}, w_B) = (0.67, 0.25, 0.4)$, and V_c given by 2^{nd} column of Table 8.

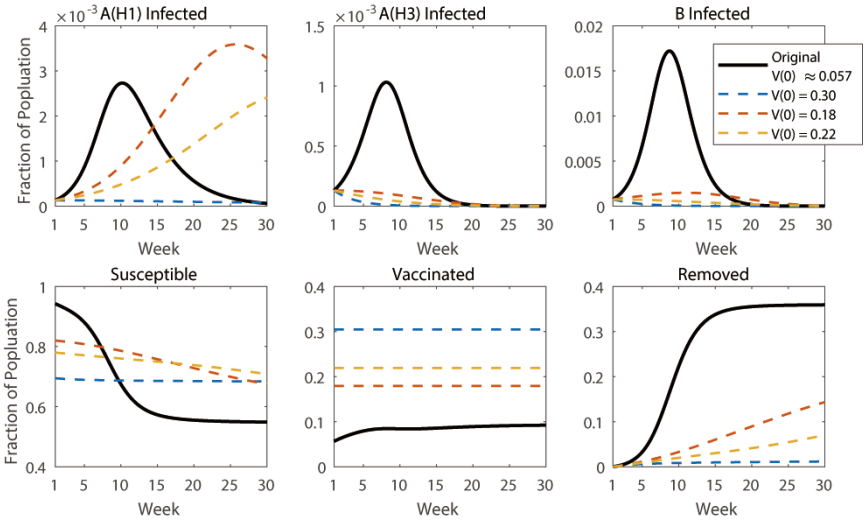

(b) $(w_{A(H1)}, w_{A(H3)}, w_B) = (1, 1, 1)$, and V_c given by 3^{rd}column of Table 8.

Figure 20: The dynamics of SVIR model 2, for different critical vaccination threshold V_c. Except the original result, it is assumed that $V(0) = V_c$ and no further vaccination took place within the period.

Subtype	V_c with baseline/original w	V_c with 100% w
A(H1)	0.45	0.30
A(H3)	0.72	0.18
B	0.55	0.22

Table 8: Critical vaccination thresholds of different influenza subtypes.

In the following, we assume for simplicity that $V(0) = V_c$ and no further vaccinations take place during the investigated time period (i.e., $r = 0$ in equation (1)). Figure 20 shows the results of model 2 (as given by equations (10)) with V_c calculated using the baseline VE (Figure 20a) and the 100% VE (Figure 20b). It is obvious that when the highest V_c is introduced, all subtypes infections die out at the beginning. Nonetheless, we observe in Figure 20 that reduced vaccination will lead to a delayed peak of infection in the influenza subtype that required the highest V_c as given by Table 8 (see the A(H3) infected panel of

Figure 20a, and the A(H1) infected panel of Figure 20b). Although the effect of vaccination from one season on the next season is not discussed in this paper, we will return to this aspect in the "Discussion and Conclusion" Section.

3.7. Changes in vaccination threshold with respect to the vaccine efficacy

Based on the results of numerical simulations in Figure 13, 15, 16 and 20, we can conclude that both vaccination coverage and vaccine efficacy needed to be higher to prevent the 2017 - 2018 influenza epidemics in Hong Kong (so as to enable the existence of herd immunity to prevent the spread of infections). Figure 20 suggested that a minimum of 72% initial population was required to be vaccinated to prevent influenza this season. This figure also suggested that only a minimum of 30% vaccinated population is needed if a perfect vaccine is introduced. Since it is generally difficult to achieve such high percentages (100% VE or 72% V(0)), we have to determine the combinations that are practically achievable.

In the following, we assume for simplicity that $V(0) = V_c$ and no further vaccination takes place within the period (i.e., $r = 0$ in equation (1)). We also assume that the VE for all subtypes are the same ($w = w_{A(H1)} = w_{A(H3)} = w_B$), and calculate (using equation (18)) the V_c of different influenza subtypes as we vary the VE. For each vaccine efficacy w, since we obtain different V_c corresponding to different R_0 for three different virus subtypes (see equation (18)), we select the highest V_c such that all infections will die out at the beginning. The results are shown in Figure 21. We observe that all other curves except the original one are more or less superimposed on top of each other, meaning that each pair (w, V_c) will lead to relatively similar results.

a)

w	50%	60%	70%	80%	90%	100%
V_c	0.61	0.51	0.44	0.38	0.34	0.3

b)

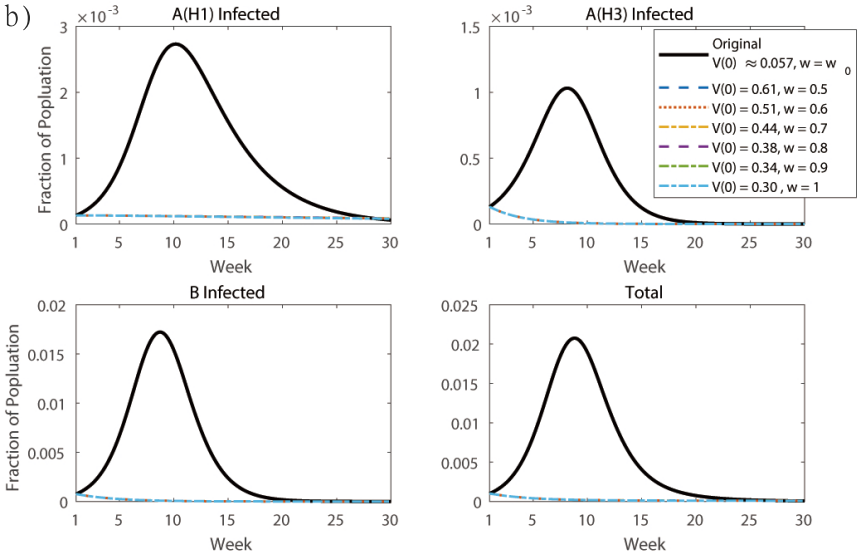

Figure 21: (a) Critical vaccination thresholds correspond to different vaccine efficacies. The highest vaccination threshold among each subtype is chosen to be the selected V_c. In equation (18), we assume that $w = w_{A(H1)} = w_{A(H3)} = w_B$ but R_0 is different for A(H1), A(H3), and B (see Table 7). (b) The dynamics of SVIR model 2, for different vaccine efficacies w and chosen critical vaccine threshold V_c as given by (a). Except the original result (i.e. $w_0 = (0.67, 0.25, 0.4)$; see Table 6), it is assumed that $V(0) = V_c$ and no further vaccination took place within the period. The VE for all subtypes are assumed to be the same, i.e., $w = w_{A(H1)} = w_{A(H3)} = w_B$.

Obviously, the vaccination threshold V_c in Figure 21 is still high compared to the current vaccination threshold in Hong Kong (see Section 2.2). For this reason, in Figure 22 we decided to investigate the dynamics of model 2 when V_c is reduced by half. In this case we observe that the peak of total infection is almost a quarter of the original peak (i.e., 0.005 vs. 0.02). These results provide an insight for research and government to decide the best vaccine strategy on the basis of vaccination coverage, vaccine efficacy and the size of epidemics.

a)

w	50%	60%	70%	80%	90%	100%
$\frac{V_c}{2}$	0.30	0.25	0.22	0.19	0.17	0.15

b)

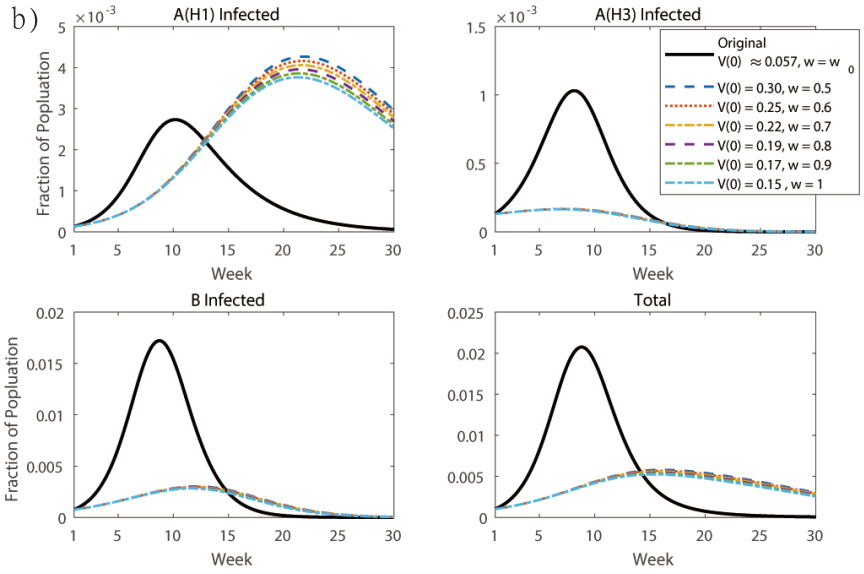

Figure 22: (a) Half of the critical vaccination thresholds V_c. (b) The dynamics of SVIR model 2, for different vaccine efficacies w and half of the critical vaccination threshold V_c as given by (a). Except the original result (i.e. $w_0 = (0.67, 0.25, 0.4)$; see Table 6), it is assumed that $V(0) = V_c$ and no further vaccination took place within the period. The VE for all subtypes are assumed to be the same, i.e., $w = w_{A(H1)} = w_{A(H3)} = w_B$.

4. Discussion and Conclusion

In this study, two mathematical models have been developed to investigate the Hong Kong influenza epidemic during the 2017 - 2018 winter based on the overall epidemic and influenza viruses' subtypes. Least squares method and bootstrap method have been used for fitting the data to the models, to estimate parameter values. Also, simple mathematical analysis has been carried out to identify the reproductive ratios for the infections in the two models, as well as the steady states and their stability.

Numerical simulations presented in this study emphasised the importance of the vaccination coverage and vaccine efficacy in preventing the spread of in-

fection (Section 3.1 and 3.3). The results showed that a perfect vaccine cannot prevent the spread because of the low vaccination coverage (Section 3.3). Also, the results suggested that the increase in the vaccine efficacy for one virus subtype may lead to an increase in the infections caused by a different virus subtype even if the total number of infections was decreasing (Section 3.4). Therefore, we had to determine the critical vaccination coverage so that infection spread could be prevented in the future. Results showed that 72% and 30% of initial population needed to be vaccinated to eliminate the infection from the beginning, for the cases of current (baseline) vaccine efficacy and perfect vaccine efficacy, respectively (Section 3.6). Since the data suggested that $\sim 11.6\%$ of the Hong Kong population was vaccinated during the winter 2017 - 2018 season, we hypothesise that more vaccines would be needed to prevent an epidemic in the future.

Because different influenza subtypes have different vaccine efficacies (and the efficacies also vary every year [38]), the only way to stop the infection spread is to select the highest critical vaccination threshold among all virus subtypes, once the vaccine efficacies are predicted. By choosing this threshold as the required vaccination coverage, it can ensure that all infections subtypes are eliminated at the beginning of the season (Section 3.7). Moreover, the numerical results have shown that the required coverage decreases with increasing efficacy.

We need to emphasise here the lack of data on cross-infection among the different influenza subtypes and on the effect of vaccination from previous seasons, which impeded us to investigate these aspects in the current study. However, in the future we plan to investigate at a theoretical level the possible effects of viral cross-infections, or the possible impact of previous vaccinations (which could lead to immune memory against similar viral antigens).

Finally, we note that one should investigate vaccine strategies in age-structured populations, since it is more beneficial to determine the critical vaccine coverage for each age group. However, as vaccine efficacy can vary between different ages and since there is a lack of data on the age-dependent vaccine efficacy, this investigation was not carried out in this study. Future research plans (which would

benefit from more detailed data collection) would consider the investigation of the optimal vaccine coverage for each age group once the vaccine efficacies are known, and the investigation of the cost-effectiveness between a higher vaccine coverage and a higher vaccine efficacy.

Acknowledgements

DH is supported by the Early Career Scheme from Hong Kong Research Grants Council (PolyU 251001/14M).

Competing Interests

The authors declare that they do not have any competing interests.

Appendix

A. Vaccines' Compositions

The Scientific Committee on Vaccine Preventable in Hong Kong reviewed the scientific evidence of influenza vaccination and recommended the use of 2 vaccines comprising the following viruses [39]:

1. Trivalent (IIV3) inactivated influenza vaccine
    - A/Michigan/45/2015 (H1N1)pdm09-like virus
    - A/Hong Kong/4801/2014 (H3N2)-like virus
    - B/Brisbane/60/2008-like virus
2. Quadrivalent (IIV4) inactivated influenza vaccine
    - Above 3 viruses
    - B/Phuket/3073/2013-like virus

Since we do not have detailed data on infections with different B strains, throughout this study we focus only on the trivalent vaccine.

B. Mathematical Analysis of Model 1

We consider the case when a single infected individual is introduced into a fully susceptible population, i.e., $I \approx 0,\ R = V = V_e = 0 \Rightarrow S \approx 1$, and therefore

$$\frac{dI}{dt} \approx \gamma I \left(\frac{\beta}{\gamma} - 1 \right).$$

We define the basic reproductive ratio as the threshold ratio that determines the decay/growth of infections:

$$R_0 = \frac{\beta}{\gamma}. \tag{19}$$

However, in many circumstances, not all individuals are susceptible to infections as some of them might have been vaccinated or might have had enough immunity to prevent the infection. In order to improve the accuracy of the approximation, one uses the effective reproductive ratio R_{0x}, which is defined as the expected number of secondary infections caused by a single infection introduced into a population made up of both susceptible and non-susceptible individuals. We consider the case when a single infected individual is introduced into a population formed of susceptible and vaccinated individuals. If we assume that $I \approx 0,\ R \approx 0, V = V_e = V_0$ with $V_0 < 1$, it leads to $S \approx 1 - V_0$, and therefore

$$\frac{dI}{dt} \approx \gamma I \left(\frac{\beta(1 - wV_0)}{\gamma} - 1 \right).$$

We thus define

$$R_{0x} = \frac{\beta}{\gamma}(1 - wV_0). \tag{20}$$

Then if $R_{0x} > 1$ the infection will spread, and if $R_{0x} < 1$ the infection will die out. Using the parameter values from Table 3, we obtain

$$R_0 = \frac{2.7516}{2.1272} \approx 1.2935$$

$$R_{0x} \approx \frac{2.7516}{2.1272}(1 - 0.45 \cdot 0.0565) \approx 1.2607 > 1.$$

Since $R_{0x} > 1$, it is clear that an influenza epidemic occurred during the study period.

The steady states of model 1 (described by equations (3)) are

$$(S, V, V_e, I, R) = (1 - V^* - R^*, V^*, A, 0, R^*)\,,$$

where $0 \leq V^*, R^*, \quad V^* + R^* \leq 1, \quad V^* \leq A$. The Jacobian matrix associated with model 1 is given by

$$\mathbf{J}(S, V, V_e, I, R) = \begin{bmatrix} -\beta I & 0 & \frac{r}{A} & -\beta S & 0 \\ 0 & -kI & -\frac{r}{A} & -kV & 0 \\ 0 & 0 & -\frac{r}{A} & 0 & 0 \\ \beta I & kI & 0 & \beta S + kV - \gamma & 0 \\ 0 & 0 & 0 & \gamma & 0 \end{bmatrix}.$$

At the steady state,

$$\mathbf{J}(1 - V^* - R^*, V^*, A, 0, R^*) = \begin{bmatrix} 0 & 0 & \frac{r}{A} & -\beta(1 - V^* - R^*) & 0 \\ 0 & 0 & -\frac{r}{A} & -kV^* & 0 \\ 0 & 0 & -\frac{r}{A} & 0 & 0 \\ 0 & 0 & 0 & \beta(1 - V^* - R^*) + kV^* - \gamma & 0 \\ 0 & 0 & 0 & \gamma & 0 \end{bmatrix}.$$

Since $-r/A < 0 \;\; \forall A, r > 0$, the only eigenvalue that affects the stability of the steady state is

$$\begin{aligned} \lambda &= \beta(1 - V^* - R^*) + \beta(1 - w)V^* - \gamma \\ &= \beta(1 - wV^* - R^*) - \gamma. \end{aligned}$$

The steady state is stable if $\lambda < 0$, i.e., if $\beta(1 - wV^* - R^*) < \gamma$.

Next, we focus on the beginning of the influenza season and assume that we are close to the disease-free steady state. Thus we consider $R(0) = R^*$ and $V(0) = V^*$, i.e.,

$$\lambda = \beta\big(1 - wV(0) - R(0)\big) - \gamma. \tag{21}$$

It is noted that the above eigenvalue can be re-written as

$$\lambda = \gamma\Big(\frac{\beta\big(1 - wV(0) - R(0)\big)}{\gamma} - 1\Big) = \begin{cases} \gamma(R_0 - 1), R(0) = V(0) = 0 & (22) \\ \gamma(R_{0x} - 1), R(0) = 0 & (23) \end{cases}$$

Considering the disease-free and fully susceptible equilibrium where $V(0) = R(0) = 0$, this equilibrium will be unstable if $\beta > \gamma$, i.e., if $R_0 > 1$. If we instead consider the disease-free equilibrium where $R(0) = 0$ and $V(0) = V_0$, this equilibrium will be unstable if $R_{0x} > 1$. Figure 23 shows the changes in the stability of λ for different vaccine efficacies w. We observe from this figure that the disease-free and fully susceptible equilibrium ($V(0) = R(0) = 0$) is always unstable for model 1. As the vaccine efficacy w increases, the vaccinated population level $V^* = V(0)$ needed to ensure stable steady states decreases (see the x-intercept of the lines $\lambda = 0$ in Figure 23). We also observe that when $w = 0.1$ and $R(0) = 0$, the disease-free equilibrium is unstable even when the whole Hong Kong population is vaccinated (i.e., $V(0) = 1$)

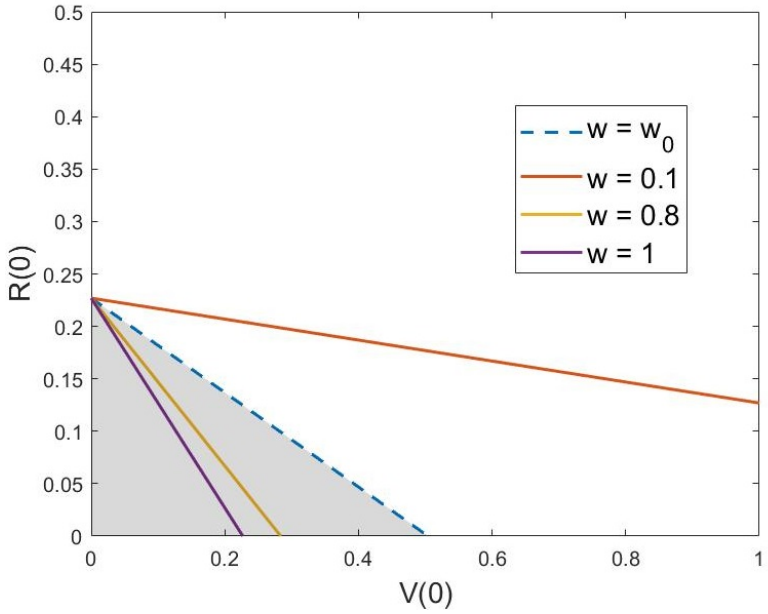

Figure 23: The dynamics, in the ($V(0)$, $R(0)$) space, of the eigenvalue λ which determines the stability of the steady states for model 1, as we vary the vaccine efficacies w. The lines represent $\lambda = 0$ for different w (see equation (21)). Parameters $\beta = 2.7516, \gamma = 2.1272$ and the baseline efficacy $w_0 = 0.45$ are as in Table 3. The shaded area represents the values of $V(0)$ and $R(0)$ where $\lambda > 0$ (unstable steady states) in the case of $w = w_0$.

C. Mathematical Analysis of Model 2

The method used to calculate the reproductive ratios in model 2 is similar to the one for model 1. If we re-arrange the differential equations for the 3 infected compartments to

$$\frac{dI_i}{dt} = \gamma I_i \left(\frac{\beta(S + (1-w)V)}{\gamma} - 1 \right), \quad i = A(H1), A(H3), B,$$

then we can consider the case when 3 individuals, each infected by one of the influenza subtype, are introduced into a fully susceptible population (i.e., $I_i \approx 0 \ \forall i, \ R = V = V_e = 0$, which allows us to approximate $S \approx 1$). Then

$$\frac{dI_i}{dt} \approx \gamma_i I_i \left(\frac{\beta_i}{\gamma_i} - 1 \right),$$

and we can define the reproductive ratios to be the following thresholds:

$$R_{0i} = \frac{\beta_i}{\gamma_i}, \quad i = A(H1), A(H3), B. \tag{24}$$

Next we consider the case when three individuals, each infected by one of the influenza subtypes, are introduced into a population formed of both susceptible and vaccinated individuals (i.e., $I_i \approx 0 \ \forall i, \ R \approx 0, V = V_e = V_0, V_0 < 1$, which allows us to approximate the susceptible population as $S \approx 1 - V_0$). Then

$$\frac{dI_i}{dt} \approx \gamma_i I_i \left(\frac{\beta_i(1 - w_i V_0)}{\gamma_i} - 1 \right).$$

Define

$$R_{0xi} = \frac{\beta_i}{\gamma_i}(1 - w_i V_0), \quad i = A(H1), A(H3), B. \tag{25}$$

The disease-free steady states for model 2 are

$$(S, V, V_e, I_{A(H1)}, I_{A(H3)}, I_B, R) = (1 - V^* - R^*, V^*, A, 0, 0, 0, R^*),$$

where $0 \leq V^*, R^*, \quad V^* + R^* \leq 1, \quad V^* \leq A$. The Jacobian matrix associated with model 2 is given by

$$\mathbf{J}(S, V, V_e, I_{A(H1)}, I_{A(H3)}, I_B, R) =$$

$$= \begin{bmatrix} -\sum_{i=1}^{3} \beta_i I_i & 0 & \frac{r}{A} & -\beta_1 S & -\beta_2 S & -\beta_3 S & 0 \\ 0 & -\sum_{i=1}^{3} k_i I_i & -\frac{r}{A} & -k_1 V & -k_2 V & -k_3 V & 0 \\ 0 & 0 & -\frac{r}{A} & 0 & 0 & 0 & 0 \\ \beta_1 I_1 & k_1 I_1 & 0 & \beta_1 S + k_1 V - \gamma_1 & 0 & 0 & 0 \\ \beta_2 I_2 & k_2 I_2 & 0 & 0 & \beta_2 S + k_2 V - \gamma_2 & 0 & 0 \\ \beta_3 I_3 & k_3 I_3 & 0 & 0 & 0 & \beta_3 S + k_3 V - \gamma_3 & 0 \\ 0 & 0 & 0 & \gamma_1 & \gamma_2 & \gamma_3 & 0 \end{bmatrix}$$

At the disease-free steady state, the Jacobian matrix reads

$$\mathbf{J}(1 - V^* - R^*, V^*, A, 0, 0, 0, R^*) =$$

$$= \begin{bmatrix} 0 & 0 & \frac{r}{A} & -\beta_1(1 - V^* - R^*) & -\beta_2(1 - V^* - R^*) & -\beta_3((1 - V^* - R^*) & 0 \\ 0 & 0 & -\frac{r}{A} & -k_1 V^* & -k_2 V^* & -k_3 V^* & 0 \\ 0 & 0 & -\frac{r}{A} & 0 & 0 & 0 & 0 \\ 0 & 0 & 0 & \beta_1(1 - w_1 V^* - R^*) - \gamma_1 & 0 & 0 & 0 \\ 0 & 0 & 0 & 0 & \beta_2(1 - w_2 V^* - R^*) - \gamma_2 & 0 & 0 \\ 0 & 0 & 0 & 0 & 0 & \beta_3(1 - w_3 V^* - R^*) - \gamma_3 & 0 \\ 0 & 0 & 0 & \gamma_1 & \gamma_2 & \gamma_3 & 0 \end{bmatrix}$$

Since $-r/A < 0 \quad \forall A, r > 0$, the only eigenvalues that are able to affect the stability of the steady state are

$$\lambda_j = \beta_j(1 - w_j V^* - R^*) - \gamma_j, \quad j = A(H1), A(H3), B. \tag{26}$$

If the inequality

$$\beta_j(1 - w_j V^* - R^*) - \gamma_j > 0$$

is satisfied for any virus subtype j, then the steady states are unstable.

D. Critical Vaccination Threshold

Herd immunity implies that if a sufficient number of individuals in a population have obtained immunity, the infection will die out without causing an epidemic. The standard herd immunity threshold for random vaccination is

$$V_c = 1 - \frac{1}{R_0},$$

where V_c stands for the critical vaccination threshold while assuming 100% VE [40]. However, it is generally difficult to obtain a perfect influenza vaccine, and thus a new equation that included the vaccine efficacy w was introduced by Plans and Rubio [37]:

$$V_c = \left(1 - \frac{1}{R_0}\right) \cdot \frac{1}{w}. \tag{27}$$

If we consider the equations (19) and (20) for R_0 and R_{0x}, we can rewrite equation (27) for V_c as follows:

$$V_c = \left(1 - \frac{1}{R_0}\right) \cdot \frac{1}{w} \quad \Leftrightarrow \quad R_0(1 - wV_c) = 1 \quad \Leftrightarrow \quad R_{0x} = 1.$$

References

[1] S. K. Peasah, E. Azziz-Baumgartner, J. Breese, M. I. Meltzer, M.-A. Widdowson, Influenza cost and cost-effectiveness studies globally – a review, Vaccine 31 (46) (2013) 5339–5348.

[2] European Centre for Disease Prevention and Control, Immunity following influenza disease and administration of influenza vaccines, accessed: 2018-06-25.
URL https://ecdc.europa.eu/en/seasonal-influenza/prevention-and-control/vaccines/immunity

[3] World Health Organization, Influenza (seasonal), accessed: 2018-06-25.
URL http://www.who.int/news-room/fact-sheets/detail/influenza-(seasonal)

[4] L. Yang, C. M. Wong, E. H. Lau, K. P. Chan, C. Q. Ou, J. S. Peiris, Synchrony of clinical and laboratory surveillance for influenza in Hong Kong, PloS One 3 (1) (2008) e1399.

[5] X.-L. Wang, L. Yang, D.-H. He, A. P. Chiu, K.-H. Chan, K.-P. Chan, M. Zhou, C.-M. Wong, Q. Guo, W. Hu, Different responses of influenza epidemic to weather factors among Shanghai, Hong Kong, and British

Columbia, International Journal of Biometeorology 61 (6) (2017) 1043–1053.

[6] Hong Kong Observatory, The Government of the Hong Kong Special Administrative Region, Climate of Hong Kong, accessed: 2018-06-25.
URL http://www.hko.gov.hk/cis/climahk_e.htm

[7] L. Yang, K. H. Chan, L. K. Suen, K. P. Chan, X. Wang, P. Cao, D. He, J. M. Peiris, C. M. Wong, Impact of the 2009 H1N1 pandemic on age-specific epidemic curves of other respiratory viruses: A comparison of pre-pandemic, pandemic and post-pandemic periods in a subtropical city, PloS One 10 (4) (2015) e0125447.

[8] A. P. Chiu, Q. Lin, E. Y. N. Tang, D. He, Anti-phase synchronization of influenza A/H1N1 and A/H3N2 in Hong Kong and countries in the North Temperate Zone, International Journal of Infectious Diseases 66 (2018) 42–44.

[9] S. Kim, J. Lee, E. Jung, Mathematical model of transmission dynamics and optimal control strategies for 2009 A/H1N1 influenza in the Republic of Korea, Journal of Theoretical Biology 412 (2017) 74–85.

[10] R. Casagrandi, L. Bolzoni, S. A. Levin, V. Andreasen, The SIRC model and influenza A, Mathematical Biosciences 200 (2) (2006) 152–169.

[11] S. M. Moghadas, C. S. Bowman, J. Arino, Competitive interference between influenza viral strains, Canadian Appl. Math. Quarterly 17 (2) (2009) 309–316.

[12] R. Omori, B. J. Cowling, H. Nishiura, How is vaccine effectiveness scaled by the transmission dynamics of interacting pathogen strains with cross-protective immunity?, PLoS One 7 (11) (2012) e50751.

[13] G. Béraud, Mathematical models and vaccination strategies, Vaccine 36 (36) (2018) 5366–5372.

[14] J. Lee, J. Kim, H.-D. Kwon, Optimal control of an influenza model with seasonal forcing and age-dependent transmission rates, Journal of Theoretical Biology 317 (2013) 310–320.

[15] I. A. Baba, E. Hincal, A model for influenza with vaccination and awareness, Chaos, Solitons & Fractals 106 (2018) 49–55.

[16] I. A. Baba, B. Kaymakamzade, E. Hincal, Two-strain epidemic model with two vaccinations, Chaos, Solitons & Fractals 106 (2018) 342–348.

[17] Respiratory Diseas Office, Centre for Health Protection, Department of Health, The Government of the Hong Kong Special Administrative Region, Surveillance data in figures in flue express, accessed: 2018-06-25.
URL https://www.chp.gov.hk/files/xls/flux_data.xlsx

[18] Respiratory Diseas Office, Centre for Health Protection, Department of Health, The Government of the Hong Kong Special Administrative Region, Flu express, Flu Express 15 (1).

[19] Respiratory Diseas Office, Centre for Health Protection, Department of Health, The Government of the Hong Kong Special Administrative Region, Flu express, Flu Express 15 (13).

[20] Census and Statistics Department, The Government of the Hong Kong Special Administrative Region, Poopulation overview, accessed: 2018-06-25.
URL https://www.censtatd.gov.hk/hkstat/sub/so20.jsp

[21] Centre of Health Protection, Department of Health, The Government of the Hong Kong Special Administrative Region, Government vaccination programme (gvp), accessed: 2018-06-05.
URL https://www.chp.gov.hk/en/features/18630.html

[22] Centre of Health Protection, Department of Health, The Government of the Hong Kong Special Administrative Region, Vaccine schemes at a glance,

accessed: 2018-06-25.
URL https://www.chp.gov.hk/en/features/18870.html

[23] Centre of Health Protection, Department of Health, The Government of the Hong Kong Special Administrative Region, Resources - seasonal influenza, accessed: 2018-06-25.
URL https://www.chp.gov.hk/en/resources/464/29.html

[24] Scientific Committee on Vaccine Preventable Diseases, Centre of Health Protection, Department of Health, The Government of the Hong Kong Special Administrative Region, Interim Consensus Statement on Use of Seasonal Influenza Vaccine in Hong Kong in Remaining Period of 2017/18 Season (2018).

[25] B. Flannery, J. R. Chung, E. A. Belongia, H. Q. McLean, M. Gaglani, K. Murthy, R. K. Zimmerman, M. P. Nowalk, M. L. Jackson, L. A. Jackson, A. S. Monto, E. T. Martin, A. Foust, W. Sessions, L. Berman, J. R. Barnes, S. Spencer, A. M. Fry, Interim estimates of 2017–18 seasonal influenza vaccine effectivenessUnited States, February 2018, American Journal of Transplantation 18 (4) (2018) 1020–1025.

[26] E. Shim, A. P. Galvani, Distinguishing vaccine efficacy and effectiveness, Vaccine 30 (47) (2012) 6700–6705.

[27] J. Tchuenche, S. Khamis, F. Agusto, S. Mpeshe, Optimal control and sensitivity analysis of an influenza model with treatment and vaccination, Acta biotheoretica 59 (1) (2011) 1–28.

[28] M. E. Alexander, C. Bowman, S. M. Moghadas, R. Summers, A. B. Gumel, B. M. Sahai, A vaccination model for transmission dynamics of influenza, SIAM Journal on Applied Dynamical Systems 3 (4) (2004) 503–524.

[29] D. He, J. Dushoff, R. Eftimie, D. J. Earn, Patterns of spread of influenza A in Canada, Proceedings of the Royal Society of London B: Biological Sciences 280 (1770) (2013) 20131174.

[30] O. Krylova, Predicting epidemiological transitions in infectious disease dynamics: Smallpox in historic London (1664-1930), Ph.D. thesis, McMaster University, Canada, Retrieved from MacSphere database (2011).

[31] G. Chowell, M. Miller, C. Viboud, Seasonal influenza in the United States, France, and Australia: transmission and prospects for control, Epidemiol. Infect. 136 (6) (2008) 852–864.

[32] N. Goeyvaerts, L. Willem, K. Kerckhove, Y. Vandendijck, G. Hanquet, P. Beutels, N. Hens, Estimating dynamic transmission model parameters for seasonal influenza by fitting to age and season-specific influenza-like illness incidence, Epidemics 13 (2015) 1–9.

[33] J. Lewnard, S. Cobey, Immune history and influenza vaccine effectiveness, Vaccines 6 (2) (2018) 28.

[34] J. Maamary, T. Wang, G. Tan, P. Palese, J. Ravetch, Increasing the breadth and potency of response to the seasonal influenza virus vaccine by immune complex immunization, Proc. Natl. Acad. Sci. 114 (38) (2017) 10172–10177.

[35] C. A. DiazGranados, A. J. Dunning, M. Kimmel, D. Kirby, J. Treanor, A. Collins, R. Pollak, J. Christoff, J. Earl, V. Landolfi, et al., Efficacy of high-dose versus standard-dose influenza vaccine in older adults, New England Journal of Medicine 371 (7) (2014) 635–645.

[36] S. M. Blower, H. Dowlatabadi, Sensitivity and uncertainty analysis of complex models of disease transmission: an HIV model, as an example, International Statistical Review/Revue Internationale de Statistique 62 (2) (1994) 229–243.

[37] P. Plans-Rubió, The vaccination coverage required to establish herd immunity against influenza viruses, Preventive Medicine 55 (1) (2012) 72–77.

[38] Centre for Disease Control and Prevention, United States, Seasonal influenza vaccine effectiveness, 2005-2018, accessed: 2018-06-05.

URL https://www.cdc.gov/flu/professionals/vaccination/effectiveness-studies.htm

[39] Scientific Committee on Vaccine Preventable Diseases, Centre of Health Protection, Department of Health, The Government of the Hong Kong Special Administrative Region, Recommendations on seasonal influenza vaccination for the 2017/18 season (2017).

[40] P. Fine, K. Eames, D. L. Heymann, Herd immunity: a rough guide, Clinical Infectious Diseases 52 (7) (2011) 911–916.